Title

ELECTRON-SPIN-RESONANCE AND CHEMICAL STUDIES OF RADIATION DAMAGE OF CHOLINE CHLORIDE AND SOME OF ITS ANALOGS

Author

Lindblom, Robert O.

Publication Date

1959-10-19

UCRL 8910

UNIVERSITY OF
CALIFORNIA

Ernest O. Lawrence
Radiation Laboratory

ELECTRON—SPIN—RESONANCE AND CHEMICAL STUDIES OF RADIATION DAMAGE OF CHOLINE CHLORIDE AND SOME OF ITS ANALOGS

DISCLAIMER

UCRL-8910
Chemistry - General

UNIVERSITY OF CALIFORNIA

Lawrence Radiation Laboratory
Berkeley, California

Contract No. W-7405-eng-48

ELECTRON-SPIN-RESONANCE AND CHEMICAL STUDIES OF RADIATION DAMAGE OF CHOLINE CHLORIDE AND SOME OF ITS ANALOGS

Robert O. Lindblom

(Thesis)

October 19, 1959

Printed for the U. S. Atomic Energy Commission

Printed in USA. Price $2.75. Available from the
Office of Technical Services
U. S. Department of Commerce
Washington 25, D.C.

RADIATION DAMAGE OF CHOLINE CHLORIDE

Contents

ELECTRON-SPIN-RESONANCE AND CHEMICAL STUDIES OF RADIATION DAMAGE OF CHOLINE CHLORIDE AND SOME OF ITS ANALOGS

Robert O. Lindblom

Lawrence Radiation Laboratory
University of California
Berkeley, California

October 19, 1959

ABSTRACT

The extreme sensitivity of choline chloride to ionizing radiation has been investigated with electron spin resonance (ESR) spectroscopy and some chemical kinetic studies. The selectively deuterated analogs of choline chloride were synthesized to aid in the interpretation of the ESR hyperfine spectrum of the radiation-produced radicals in choline chloride. The hyperfine structure was found consistent with a radical structure of : $CH_2 \cdot CH_2 - OH$. These radicals were then related to the radiation damage rate by means of kinetic studies on the radical decay, and the radiation damage rates. A 3/2-order decay rate was observed for the radical disappearance rate. A chain-decomposition mechanism has been proposed to account for this 3/2 order, and the integrated rate law has been compared with the choline decomposition rate. The model requires the observed radical to be in the form of a stabilized radical rather than the chain-propagating species. A new ESR standard was developed for the kinetic studies. It consists of a dilute solution of Mn^{+2} in a superpure MgO matrix. Since its spectrum is nearly clear at G = 2.0023, it is particularly convenient for use with radicals centered there.

INTRODUCTION

The unusual aspects of the radiation damage reaction of choline chloride were first observed by the Bio-Organic Chemistry Group at the Lawrence Radiation Laboratory in 1953.[1] Choline chloride had been synthesized with a C^{14} label in a N-methyl position, and with a specific activity of 13 microcuries per milligram. It was found to be 60% decomposed by its self-irradiation after 6 months' storage in an evacuated container at room temperature. Since the self-decomposition of most organic compounds labeled with this level of specific activity would be only a few tenths of a percent per year, this high rate of decomposition excited a great deal of interest. Quantitatively, this self-irradiation sensitivity value was G = 490. (The G value is defined as the number of molecules destroyed per 100 electron volts absorbed.) The normal range of G values for nonvinyl compounds is from 0.1 to 10.[2, 3]

This interest was intensified by the biological importance of choline and its derivatives. They are well established as vital components in human metabolism, and are to be found throughout the body.[4, 5] Choline is found as a part of a number of different lipids, and is assigned the role of a transmethylating agent by which the body completes the synthesis of methionine from homocysteine. Although choline is a much weaker vasodilator than acetylcholine, both are active materials. Acetylcholine is assigned the important role of the chemical transmitter that couples the motor nerve impulses to the voluntary muscles.

When the high radiation sensitivity of choline chloride was first observed, the possibility that radiation damage of choline could be an important factor in radiation sickness was considered. Later work showed that only crystalline choline chloride showed anomalously high radiation sensitivity, and the radiation sensitivity of choline in solution corresponded to a G value of only 3.[6] Although it is not wise to draw conclusions about *in vivo* reactions from *in vitro* experiments, these results do make the involvement of choline chloride in radiation sickness seem improbable.

The radiation sensitivity of nineteen different choline analogs has been investigated by Lemmon et al.[6] in an effort to find structural features that could be related to the anomalous radiation sensitivity of choline chloride. Although a wide selection of different anions was tried, and the methyl and ethanol groups were replaced with a wide variety of similar and differing groups, only the choline bromide showed an interesting sensitivity. Its G value was about one-third that of choline chloride.

Another interesting feature of the radiation damage of choline chloride is the deferred radiation damage reported in this same paper.[6] The effective half life for the radiation-induced chain decomposition of choline chloride is about 4 hours at room temperature. If it is examined immediately after irradiation, little damage is observed. The radiation damage can be deferred indefinitely at 77° K, and then occurs in the usual manner when the sample is allowed to warm up to room temperature.

Serlin has reported that radiation damage in choline chloride is dependent on temperature.[7] His work shows an increasing G value for choline chloride with increasing temperatures up to 50° C, and an abrupt drop in G value somewhere in the range of 50° to 150°. Later, Collin reported a phase transition at 73° to 78° in which the choline chloride went from orthorhombic to face-centered cubic,[8] and suggested--as he concluded from the appearance of his choline chloride--that the cubic phase was responsible for the radiation protection observed by Serlin.[7]

The high G value and deferrable character of the radiation damage of choline chloride make this reaction a unique study in the field of radiation chemistry. Since choline chloride is stable to thermal decomposition at temperatures up to about 200°, a minimum thermal activation energy of the order of 1.0 ev for thermal decomposition is indicated. The observation of reaction with much smaller average energies in radiation decomposition can only be interpreted as evidence for a chain-decomposition mechanism.

IRRADIATION METHODS AND DOSIMETRY

The two types of radiation sources used in these studies of irradiated choline chloride were a cobalt-60 γ-ray source and an electron linear accelerator.

Gamma Irradiations

The cobalt-60 source was used only where small irradiation effects were being investigated and where it was thus important that the samples receive identical irradiation treatment. The Co^{60} source consisted of a rotating stage surrounded by 16 concentric Co^{60} rods.[9] To assure maximum uniformity the sample tubes were arranged concentrically around the periphery of the rotating stage and all the samples used in one experiment were exposed simultaneously. The dose was calculated from the exposure time and the dose rate. The latter had previously been determined with ferrous sulfate dosimetry.[9] Although the dose rate from the Co^{60} source could be adjusted by changing the radial position of the Co^{60} rods, it lacked the range and flexibility of the linear accelerator, from which a wide range of doses could be delivered. At the time these experiments were done there was no way to control the temperature in the Co^{60} source, so that the samples could not be irradiated at -170° and consequently the samples were changing composition during the irradiation. Since Lemmon et al.[6] had shown a half time for decomposition at room temperature of 4 hr, only a small amount of decomposition should occur during the 15-min irradiation period customarily used.

The same diffuse and penetrating fields in the Co^{60} source that make possible identical radiation doses also cause a difficult complication in ESR measurements. The whole sample tube develops F centers and other radiation damage. The signals from these centers then override and obscure the signal from the irradiated sample. One way to circumvent this problem is to anneal the upper end of the evacuated sample tube while cooling the lower end, containing the sample, in liquid N_2. This procedure was used by Lemmon et al.[6] Apart from the obvious difficulty of controlling the temperature so that it was high enough to anneal but not so high that the tube collapsed, this procedure

gave erratic ESR-observed radical stability. This variability appears to be due to small amounts of thermal decomposition products formed on the heated walls during the annealing process. A radical signal observed in an irradiated tetramethylammonium chloride sample disappeared overnight after thermal annealing, although it had previously shown no observable reduction in radical concentration over a 4-month period.

Electron Irradiations

The problem of F centers in the glass was avoided by using the linear accelerator to irradiate samples for ESR experiments. This allowed irradiation of the sample in only 6 mm of one end of the tube; the other end, not irradiated, was thus left free of F centers and the sample could later be slid down into it for the ESR examination. A 4.5-Mev linear electron accelerator was used for most of the irradiations. Although the accelerator and auxiliary equipment have been described in some detail,[10] some changes worth noting were made before this work was done. A permanently installed metal well has been substituted in the vacuum chamber for the glass sample holder. The well has two thin aluminum windows for the passage of the electron beam and a Dewar tube to deliver cooling gas to the parts of the sample and holder that are in the electron beam. Cooling gas was obtained by evaporating liquid nitrogen in a Dewar vessel and piping it in Dewar tubes to the well. The use of a well permits efficient cooling of the sample and allows a rapid change of samples. Samples of 5 to 10 mg of choline (sealed in evaculated 3-mm o. d. Pyrex tubes) could be irradiated at -170° at a dose rate of about 10 megarads a minute with less than 5° temperature rise during irradiation. The linear accelerator delivered 6-μsec pulses of 4.5-Mev electrons. The electron beam's cross section was slightly elliptical and about 1 cm^2 in area. Although the pulse time was fixed, the pulse rate and current were variable. Most of the runs were made with a pulse rate of 30 pps and an average current of 0.133 μa. To assure a relatively monoenergetic beam, an electromagnet was used to bend the beam through a set of collimators. The geometry of this monochromator limits the energy spread in the

electrons to ± 5% of the 4.5-Mev value. The beam emerged from the vacuum chamber through a thin aluminum foil into the nitrogen-cooled sample well at -170°. After penetrating the sample, the beam left the well through another foil, went back into the vacuum, and was absorbed in an insulated Faraday cup. The current thus collected was measured with an electronic integrator.

Dose and G-value Calculations

The dose in megarads (10^8 ergs per gram) is easily derived from Feather's Rule, $R = 0.52\ E - 0.160$, which relates the target range R (in g/cm^2) of an energetic electron (above 0.8 Mev) to the energy lost (in Mev) in passage through the target. The radiation dose (megarads = 10^8 ergs/g) and G-value formulas:

$$D_m = 0.185\ Q_s,$$

where D_m = radiation dose in megarads,

Q_s is microcoulombs per cm^2 of beam cross section,

$$G = \frac{P(69.0)(139.6)}{(D_m)(\text{mol wt})},$$

P = % decomposition of the sample,

D_m = dose in megarads,

mol wt = molecular weight of the quaternary salt.

(These are derived in Appendices I and II.)

Since the geometry is fixed, the dose is just proportional to the surface density put through the sample. This charge rate can easily be adjusted and the integrated charge measured over a very wide range. By using the linear accelerator, a set of six samples can easily be irradiated with doses from 72 megarads to 7.2 kilorads in 2 hours' time with a dose-estimation error of ± 10%. (This variation is due to play in the sample holder.)

CHEMICAL ANALYSES

Three procedures have been used to determine the extent of decomposition of irradiated choline chloride and its analogs: reineckate analysis, sodium tetraphenylboron analysis, and a volatile-amine analysis. The volatile-amine analysis evolved later than the reineckate and sodium tetraphenylboron analyses, and has, to a large extent, superseded them in the study of radiation damage to choline and its analogs. The reineckate and the sodium tetraphenylboron analyses are measures of the undamaged quaternary starting material, whereas the volatile-amine method measures a product of the decomposition. It is desirable to keep the radiation damage low so that the sample composition during the irradiation is well known. In this work, the radiation damage was kept at less than 15%. Requiring that the radiation damage be small greatly limits the accuracy of the reineckate and the sodium tetraphenylboron procedures, as, in both these methods, the radiation damage is found as a small difference between two large measured values. The amine-diffusion method is far more accurate, since it measures directly a radiation-damage product. The sodium tetraphenylboron analysis was used on trimethyl-3-hydroxy-propyl-ammonium chloride, as the reineckate salt of this material was too soluble in propanol to allow proper washing of the precipitate.

Reineckate Analysis

The reineckate analysis--approximately the same procedure as that of Glick[11]--is detailed as follows:

1. Accurately weigh out about 10 mg of sample and make up to a volume of 10 ml with water in a volumetric flask.
2. Pipet a 3-ml aliquot into a 25-ml beaker and add 10 ml of water and 1 drop of 50% NaOH solution.
3. Boil 15 minutes to remove the volatile amine.
4. After cooling, neutralize with 4 or 5 drops of 7 N HCl to about pH 7.
5. Add 5 ml of freshly prepared 2% ammonium reineckate in methanol.

6. Cool 30 min in a freezer or 24 hr in a refrigerator; then filter on a medium sintered-glass filter funnel.

7. Wash out the excess ammonium reineckate with three 1-ml portions of n-propanol.

8. Dissolve in acetone and QS to 5 ml.

9. Measure the optical density at 526 millimicrons and calculate the amount of quaternary, using $E_{526} = 110$, i.e.,

$$\text{fraction decomposed} = \left(\frac{10}{3}\right)(5)\left(\frac{OD}{110}\right)(\text{mol wt})/S,$$

where OD = the optical density of the solution in Step 9;

mol wt = the molecular weight of the quaternary salt analyzed;

S = sample weighted out initially, in mg.

Sodium Tetraphenylboron Analysis

The sodium tetraphenylboron analysis follows the procedure of Marquardt and Vogg,[12] and is as follows:

1, 2, 3. These steps are the same as for the reineckate analysis.

4. Neutralize with HOAc to pH 4 to 6.

5. Add excess 0.1 N sodium tetraphenylboron and refrigerate overnight.

6. Filter and then wash with cold water containing a few drops of HOAc.

7. Dry over P_2O_5 in a vacuum desiccator, and weigh.

8. Calculate the decomposition with

$$P = \left(W\right)\left(\frac{10}{3}\right)\left(\text{mol wt}\right) \times 100/(C + 319)S,$$

where P = % decomposition of the quaternary, W = weight of dried precipitate, mol wt = molecular weight of the quaternary tested, S = original sample weight taken, C = formula weight of the quaternary cation.

Trimethylamine Analysis

In an earlier publication by Tolbert et al. the major products of radiation damage in choline chloride were identified as acetaldehyde and trimethylamine. Tolbert and co-workers also showed, with paper chromatography and a C^{14} label in the N-methyl position, that the radioactivity on the paper could be quantitatively accounted for by the activities in the trimethylamine product and in the undamaged choline chloride.[1] This work, together with the high G values of choline, indicates that the trimethylamine hydrochloride product is an excellent index of the radiation damage. The use of an amine-diffusion method avoids errors due to other acidic components which would titrate along with the amine hydrochloride in a direct titration. Aside from the advantage of being well established as a damage index by Tolbert's work, the trimethylamine is conveniently fixed in solution as its hydrochloride until it is volatilized by the saturated sodium carbonate and reabsorbed by the aliquot of sulfuric acid in cup C of the diffusion cell, as illustrated in Fig. 1. In this way no evaporation losses occur in the handling of the irradiated choline chloride.

The procedure for trimethylamine is as follows:

1. A sample of approximately 5 mg is transferred to a small test-tube-shaped weighing tube that just slips over the open irradiation tube so that air contact is minimized in the weighing procedure.

2. The sample is dissolved in 100 microliters of water.

3. An aliquot (10 μl or more) is transferred to point B of the Tompkin-Kirk diffusion cell as shown in Fig. 1.

4. Two hundred μl of saturated Na_2CO_3 is added at point A and a 50-μl aliquot of 0.1 $\underline{N}$ H_2SO_4, containing methyl red indicator, is added to cup C.

5. The cell is closed and evacuated through D. The cell pressure is lowered until the first evidence of boiling is seen in cup C. Then, the cell is sealed by pulling out D until the orifice is just outside the stopper.

6. The base is mixed with the sample and an hour is allowed for diffusion.

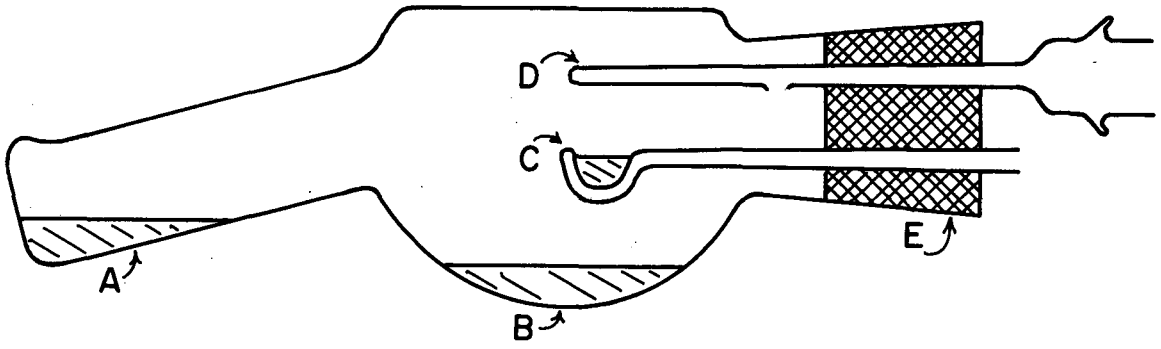

Tompkin-Kirk Diffusion Cell

MU-16369

Fig. 1. Diffusion cell for volatile-amine analysis.

7. The vacuum is released gently and the sample is titrated to the methyl red end point.

8. The percent decomposition is calculated from

$$P = \frac{(A-T)\ 139.6\ (100 + S)\ (100)}{S \quad L}$$

where P = % decomposition,

A = acid aliquot in cup C, in moles,

T = back titration in moles,

S = original sample weight,

L = aliquot of sample used in step 3.

SYNTHESIS AND USE OF DEUTERIUM-LABELED COMPOUNDS

Introduction

The synthesis and use of deuterium-substituted compounds to assist in the assigning of spectral features to vibrational and rotational modes of organic molecules has been common in infrared (ir) and microwave spectroscopy for many years. Its use with vibrational spectra in the ir predates ESR spectroscopy. General reviews appeared in 1947 and again in 1951.[13, 14] The deuterated analog of a compound differs greatly from the undeuterated compound in its ir vibrational spectrum, microwave spectrum, and ESR spectrum. Its reaction kinetics may also be significantly altered, but, in general, it remains structurally very similar to the original compound. The use of deuterated analogs in ESR spectroscopy is almost entirely parallel to their use in ir spectroscopy, although in ESR spectroscopy the atomic masses and the vibrational modes they undergo are of no concern. Instead, hyperfine ESR structure due to interaction of the proton spin moments with an electron gives rise to the important spectral features whose assignment is of concern. The deuterium nucleus has a spin moment (M_i) of 1 unit ($\hbar$), which is twice the value of the hydrogen nucleus. However, the magnetic moment (μ) of the deuterium nucleus is much smaller than that of the hydrogen nucleus. Deuterium's value is 0.875 nuclear magnetons (nm) and hydrogen's value is 2.793 nm. The number of hyperfine lines for an electron interacting with n equivalent nucleons is equal to $(2nM_i + 1)$. The amount of splitting is proportional to both M_i and μ_i. The effect of a deuteration on the ESR hyperfine spectra of a radical is to increase the number of lines by from 1-1/2 to 2 times (depending on n) and to decrease the splitting to about 60% of the value of the undeuterated compound. When the resolution is incomplete with the undeuterated compound, deuteration usually causes a complete loss of the hyperfine structure. Deuteration can be used to reveal which protons (or combination of protons) in a molecule are responsible for the hyperfine structure of a radical. When the product and starting material are well known, this can often indicate some of the structural features of the radical intermediate.

The replacement of a hydrogen by a deuterium atom is easily done on those sites that exchange rapidly, for example, the hydrogens in -O-H, -N-H, or ≡C-H groups. In general, selective deuteration of other sites poses a considerable synthetic problem. This is probably the reason that relatively little use of isotopically substituted molecules has been made in ESR work with organic radicals. In the recent literature there are many papers on the application of ESR to radiation-damage studies. A few of these have used the deuterium-substitution approach. A typical example of the use of deuterium in an easily exchangeable system is the study of trapped hydrogen atoms in irradiated frozen acids by Livingston et al.,[15] or the similar work on frozen H_2O_2 by Matheson and Smaller.[16] Alger et al.[17] studied the radicals produced by irradiating a series of frozen alcohols and alkanes. A good example of a nonexchangeable deuterated analog is in this work. They included the ESR spectra of CD_3OH in their work. The spectra indicate CD_2-OH as the trapped radical. Unfortunately, this work was not extended to any other compounds whose deuterated analogs were not commercially available, although it is for the more complicated molecule that the technique is most useful and necessary. Adam and Weissman have synthesized triphenylmethyl enriched with C^{13} in the methyl position and used it to measure the spin density at the methyl position.[18] This is an excellent example of the use of isotopes other than deuterium to interpret and analyze ESR spectra. More typical studies of organic radicals are those of Adams et al. on quinone redox reactions,[19] or those of Gordy et al., who have studied the spectra of irradiated crystalline organic solids,[20] or Smaller and Matheson, who have studied the spectra of irradiated frozen non-crystalline organic compounds.[21] To only a very few of the spectra in these papers can definite radical structures be assigned and even these are not completely unambiguous. In every case, at least for the simple, pure chemicals, the structure of the starting material is well known. Sometimes the reaction products are known either from the authors' work or the work of a previous investigator. Treatment with radiation, oxidation, or reduction--whichever is applicable--produces

radicals, and their ESR spectra are obtained. Occasionally the product, the radical spectrum, and the starting material are all consistent with only one radical intermediate. Much more often, either the spectrum is too complex for simple interpretation or the spectral features do not have the predicted intensity distributions and the authors present the data only as a "fingerprint" of an unknown radical. Selective deuteration and more detailed product analysis are both needed to allow structural assignments to be made for radical intermediates whose structure is either uncertain or completely unknown. A more detailed structural knowledge of the organic radicals should greatly contribute to our knowledge of their role in chemical reactions.

Reviews of the Synthesis of Deuterium-Labeled Compounds

There have been a number of valuable reviews on the synthesis and applications of deuterium- and tritium-containing compounds,[22, 23, 24, 25] The review by Murray and Williams[22] is the most complete and useful of these references.

Unsuccessful Exchange Reactions

The exchangeability of the four different proton positions of choline is of interest from two points of view. If a position exchanges readily with D_2O, then an exchange technique is the simplest way to get choline deuterated in that position; secondly, in any synthetic procedure one has to take into consideration the possibility of a back-exchange reaction with solvents. Also, if more than one position exchanges readily, then these positions will not be easily distinguishable.

Only the hydroxy proton was known to be easily exchanged. Therefore, the exchange of the other positions was investigated with choline chloride, trimethylamine hydrochloride, and ethanolamine hydrochloride. The samples were put in NMR tubes as 30% solutions in 0.2 M NaOD and as 50% solutions in 12 M DCl. Although the samples were heated as high as 130° for two days no exchange of H bound to C with the solvent was observed with NMR. Only decomposition of choline chloride in the acid-catalyzed tubes and attack on the glass in the base-catalyzed samples was apparent. Although these experiments failed to show any easy exchange route to selectively deuterated choline

chlorides, they did show that synthetic deuterated choline chlorides would be stable to loss of deuterium by exchange with the solvent, under most reaction conditions.

Unsuccessful Urethane Reductions

Since the early workers believed that trimethylamine was involved in the chain-transfer step of radiation-induced choline decomposition, the first attempts at deuteration were for the N-methyl positions. The following route has been utilized by Dannley, Luken, and Shapiro[26] to synthesize methyl-substituted amines in yields of 80% to 96%:

$$(Bu)_2NH + ClCOOEt \longrightarrow (Bu)_2NCOOEt \xrightarrow{LiAlH_4} (Bu)_2NCH_3 .$$

Since this work indicated that $LiAlH_4$ could, in some cases, reduce urethanes all the way to methylamines, an attempt was made to synthesize trimethylamine-d_9 from ammonia by multiple reactions with ethyl chloroformate and reductions with $LiAlH_4$ as follows:

$$NaOH + NH_3 + ClCOOEt \longrightarrow NH_2COOEt \xrightarrow{LiAlD_4} NH_2CD_3 \quad (1)$$

$$CD_3NH_2 + ClCOOEt \longrightarrow CD_3NHCOOEt \xrightarrow{LiAlD_4} CD_3NHCD_3 \quad (2)$$

$$(CD_3)_2NH + ClCOOEt \longrightarrow (CD_3)_2COOEt \xrightarrow{LiAlD_4} (CD_3)_2NCD_3 \quad (3)$$

Although the urethane synthesis went in 85% yield, the first reduction step failed and no volatile base could be found in the reaction mixture. The reduction was attempted at temperatures from 0° to 35° in ether, 65° in tetrahydrofuran, and 100° in tetrahydrofurfuroxytetrahydropyran.

Unsuccessful Reduction of Propylene Carbonate to Deuteromethanol

Hill et al.[27] have successfully reduced ethyl heptanoate to the terminally deuterated alcohol:

$$C_6H_{13}COOEt \xrightarrow[\text{in ether}]{\overset{Na}{\underset{AcOD}{}}} C_6H_{13}CD_2OD$$

On the basis of this reaction an effort to reduce propylene carbonate with sodium was tried:

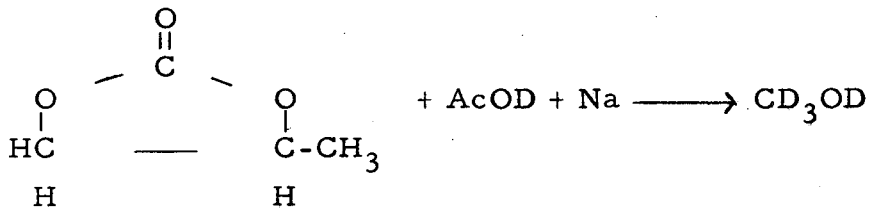

No low-boiling products could be distilled from the viscous reaction mass that resulted from adding sodium to a solution of acetic acid-d_1 and propylene carbonate in ether.

Acetic Acid-d_4 from Carbon Suboxide

Acetic acid-d_4 is a very useful intermediate for the synthesis of deuterated compounds. Wilson[28] has described the hydrolysis of carbon suboxide with D_2O to malonic acid-d_4, and the decarboxylation of the malonic acid to acetic acid-d_4:

$$O{=}C{=}C{=}C{=}O + D_2O \xrightarrow[\text{ØH}]{} DOOCCD_2COOD,$$

$$DOOCCD_2COOD \xrightarrow[150^\circ]{\text{vacuum}} CD_3COOD.$$

Carbon suboxide can be made by dehydrating malonic acid with P_2O_5, and the original synthesis was by this route.[29] However, the pyrolysis of diacetyl tartaric anhydride gives better yields, 39-50%, from cheaper starting materials:[30]

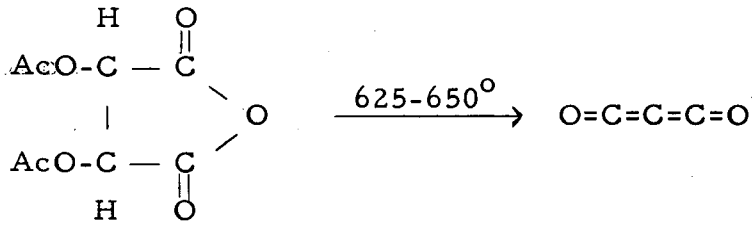

This route to acetic acid-d_4 was investigated through the malonic acid. A 32% yield was obtained in spite of some difficulties with the pyrolysis furnace. The furnace tube was made of Pyrex. It sagged in operation and cracked on cooling. The use of a furnace tube of Pyrex 1720 or, better yet, of Vycor or some other high-silica glass would eliminate these problems. The thermal decarboxylation step from malonic acid to acetic acid was no longer carried out when commercial acetic acid-d_4 became available at $3 to $10 per gram.[31]

Useful Routes in the Synthesis of Selectively Deuterated Choline Chloride

Two synthetic routes based on the acetic acid-d_4 and one based on a $LiAlD_4$ reduction, along with a simple exchange reaction, served to synthesize the selectively deuterated choline chlorides needed for the ESR studies. These reactions, numbered to correspond to a numbering system for the nonequivalent proton positions of choline chloride, are shown in Table I. The detailed synthesis will be discussed in the following paragraphs. The deuterated cholines were characterized by their C and H analyses (Table II) and by their nuclear magnetic resonance (NMR) spectra. (These C and H analyses are tabulated in Table II and the NMR spectra are shown in Fig. 5.)

Route 1: The Silver Salt Reaction to $(CD_3)_3\overset{+}{N}CH_2CH_2OH\ Cl^-$

The first portion of this route is the so-called silver salt, or Hunsdiecker, reaction.[32] No detailed procedures for making methyl bromide are available, although Hunsdiecker has a patent covering this reaction. The ultimate use of refluxing CCl_4 as a solvent for this reaction and gradual Br_2 addition was adopted as the result of difficulty in controlling the reaction. When all the reactants were added at -10° in CCl_4 no reaction occurred until the reactants warmed up a few degrees. Then, a very rapid decarboxylation occurred and joints were blown apart and the products lost. This problem was resolved by using the procedure of Dauben and Tilles,[33] which consisted of adding the Br_2 as a solution in CCl_4 to a slurry of the silver salt in refluxing

Table I

Synthetic and exchange routes to selectively deuterated choline chlorides.
(Designations for nonequivalent proton positions in choline chlorides:

$[(CH_3)_3NCH_2CH_2OH]^+Cl^-$
1 2 3 4)

Route No.	
1	$CD_3COOD \xrightarrow{AgOH} CD_3COOAg \xrightarrow{Br_2} CD_3Br \xrightarrow{NH_2CH_2CH_2OH} (CD_3)_3\overset{+}{N}CH_2CH_2OH\ Br^-$ $\xrightarrow{\text{ion ex. } Cl^-} (CD_3)_3\overset{+}{N}CH_2CH_2OH\ {}^+Cl^-$
2	$CD_3COOD \xrightarrow{Br_2} \xrightarrow{BzBr} \xrightarrow{EtOH} CD_2BrCOOEt \xrightarrow{(CH_3)_2NH} (CH_3)_2NCD_2COOEt$ $\xrightarrow{LiAlH_4} (CH_3)_2NCD_2CH_2OH \xrightarrow{CH_3I} (CH_3)_3\overset{+}{N}CD_2CH_2OH\ I^- \xrightarrow{\text{ion ex. } Cl^-}$ $(CH_3)_3\overset{+}{N}CD_2CH_2OH\ Cl^-$
3	$CH_3COOH \xrightarrow{Br_2} \xrightarrow{BzBr} \xrightarrow{EtOH} CH_2BrCOOEt \xrightarrow{(CH_3)_2NH} (CH_3)_2\overset{+}{N}CH_2COOEt\ Br^-$ $\xrightarrow{LiAlD_4} (CH_3)_2NCH_2CD_2OD \xrightarrow{CH_3I} \xrightarrow{\text{ion ex. } Cl^-} (CH_3)_3\overset{+}{N}CH_2CD_2OD\ Cl^-$
4	$(CH_3)_3\overset{+}{N}CH_2CH_2OH\ Cl^- \xrightarrow{D_2O} (CH_3)_3\overset{+}{N}CH_2CH_2OD\ Cl^-$
3a	$(CH_3)_3\overset{+}{N}CH_2COOH\ Cl^- \xrightarrow{Ag_2O} (CH_3)_3N^+CH_2COO^- \xrightarrow{310^\circ} (CH_3)_2NCH_2COOMe \xrightarrow{LiAlD_4}$ $(CH_3)_2NCH_2CD_2OD \xrightarrow{MeI} (CH_3)_3\overset{+}{N}CH_2CD_2OH\ I^- \xrightarrow{\text{ion ex. } Cl^-}$ $(CH_3)_3\overset{+}{N}CH_2CD_2OH\ Cl^-$
3b	$CH_3COOH \xrightarrow{PBr_3} \xrightarrow{Br_2} \xrightarrow{EtOH} CH_2BrCOOEt$

Table II

C and H analysis of deuterated choline chlorides

Element	Weight	% Composition Expected	Found
$(CH_3)_3\overset{+}{N}CH_2CH_2OH\ Cl^-$			
C_5	60.05	43.006	43.1
H_{14}	14.11	10.10	10.3
D_0	0	0	
N	14.01		
O	16.00		
Cl	35.46		
	139.63		
$(CH_3)_3\overset{+}{N}CH_2CD_2OH\ Cl^-$			
C_5	60.05	42.40	42.5
H_{12}	12.10	11.38	11.3
D_2	4.02		
N	14.01		
O	16.00		
Cl	35.46		
	141.64		
$(CD_3)_3\overset{+}{N}CH_2CH_2OH\ Cl^-$			
C_5	60.05	40.38	40.5
H_5	5.04	15.59	14.9
D_4	18.14		
N	14.01		
O	16.00		
Cl	35.46		
	148.70		
$(CH_3)_3\overset{+}{N}CD_2CH_2OH\ Cl^-$			
C_5	60.05	42.40	42.5
H_{12}	12.10	11.38	11.5
D_2	4.02		
N	14.01		
O	16.00		
Cl	35.46		
	141.64		
Impure 2nd Crop			
$(CH_3)_3\overset{+}{N}CD_2CH_2OH\ Cl^-$			
C_5	60.05	42.4	42.7
H_{12}	12.10	11.38	11.2
D_2	4.02		
N	14.01		
O	16.00		
Cl	35.46		
	141.64		
Hypothetical Impurity in 2nd Crop			
$(CH_3)_2N(CD_2CH_2OH)_2$			
C_6	72.06	43.0	
H_{11}	11.10	9.2	
D_4	4.02		
N	14.01	8.4	
O_2	32.00	19.2	
Cl	35.5	21.2	
	167.68		

CCl_4 solution. The condensation and quaternization of the MeBr-d_3 with $NH_2CH_2CH_2OH$ were run as a single step, with Na_2CO_3 as the base. Possibly better yields could have been obtained if this condensation had been run as three steps, with the methylated amines liberated as separate steps between condensations. This would minimize any side reaction between Na_2CO_3 and MeBr-d_3.

Route 1: Synthetic Procedure

Seven milliliters (9.2 g) of AcOH-d_3 was neutralized with 5.7 g of NaOH dissolved in 25 ml of H_2O. This solution of NaOAc-d_3 was added to a stirred solution of 24.2 g of $AgNO_3$ in 50 ml of H_2O. The filtered precipitate of AgOAc-d_3 was washed four times with 50-ml portions of H_2O. When the combined filtrates were reduced to 50 ml volume on a steam bath, an additional 4.8 g of AgOAc was recovered. The combined AgOAc-d_3 weighed 21.4 g after drying in a vacuum oven at 60° and 150 mm Hg. The silver salt reaction was run in the apparatus sketched in Fig. 2. A slurry of 21.4 g of AgOAc-d_3 with 250 ml of CCl_4 was added to the 500-ml flask. To insure dryness, a few milliliters of CCl_4 was boiled off. A mixture of 8 ml of Br_2 (P_2O_5-dried) in 50 ml of dry CCl_4 was added cautiously to the refluxing slurry of AgOAc-d_3. After a few seconds the reaction started and the bulk of the bromine was added at such a rate that vigorous gas evolution was maintained. About 8.6 g of MeBr-d_3 was made and collected in the dry-ice trap. This was a 70% yield based on the AgOAc.

About 7 ml (11.9 g) of MeBr-d_3 was distilled into a stirred solution containing 2.7 g (2.6 ml) of ethanolamine and 20 g of K_2CO_3 in 50 ml of ethanol. The equipment for this reaction is shown in Fig. 3. The reaction is rapid and quite exothermic, so that the cold finger is necessary to control the temperature and prevent loss of the MeBr-d_3. From this reaction, 5.8 g of crystalline product was recovered as a crude choline bromide.

Two grams of this crude choline bromide was changed to the chloride by putting it through a column of Dowex 1-×8 resin in a 2-by-17-cm column (approximately 100 milliequivalents of chloride capacity). By evaporation and crystallization 0.769 mg of $(CD_3)_3NCH_2CH_2OH^+ Cl^-$

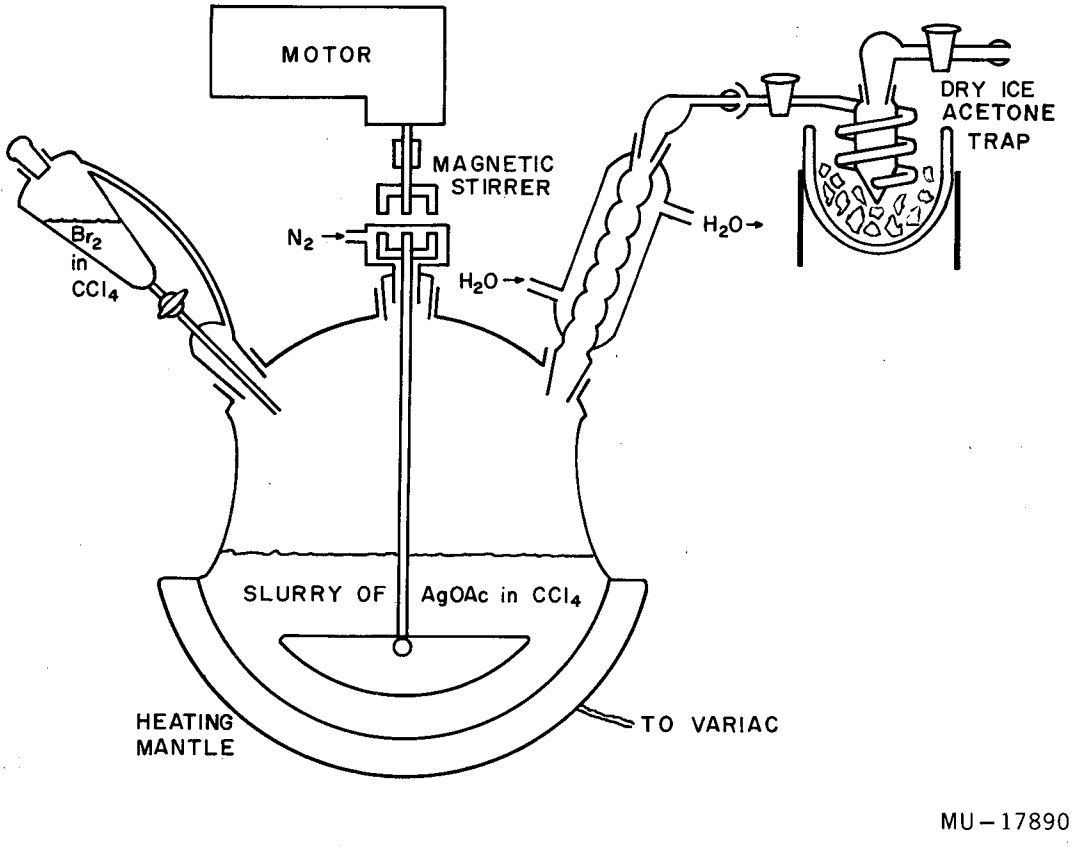

Fig. 2. Apparatus for the silver salt reaction.

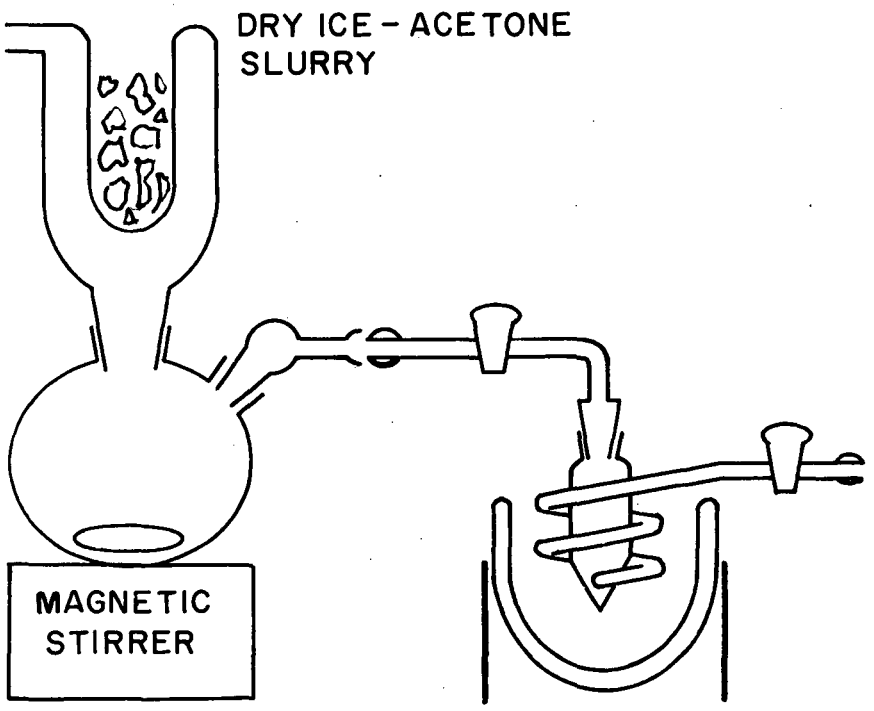

Fig. 3. Apparatus for the quaternization of ethanolamine.

was recovered. This represents a 40% yield in the combined quaternization and ion-exchange steps. The net yield of the whole synthesis was 25.4% based on the initial HOAc-d_4. The product was characterized by C and H analysis and by its NMR spectra. These data are summarized in Table II and Fig. 5.

Routes 2, 3, and 4: Deuteration in the Ethanol Portion of Choline

These reactions have a number of steps in common, and will be discussed as a group. Several different methods were used to get the ethyl ester of N, N-dimethyl glycine. The synthesis of bromoacetyl bromide has been run as a one-step reaction with P and Br_2 on a large scale by Arens and Van Dorp[34] with a 68% yield. However, my first attempts at this reaction were run as a two-step reaction with PBr_3 and Br_2, as shown in Route 3b in Table I. The yield of $BrCH_2COBr$ was 63%. A simpler method that minimizes material transfers and gives a much better yield was developed with benzoyl bromide used to convert the acid or bromoacid to the acid halide. Either the acid halide formation or bromination steps can be done first. Bromoacetyl bromide yields of 85-90% were achieved by using Route 3, Table I.

The esterification step was extremely sensitive to the order of reagent addition. It was essential to add the alcohol to the bromacetyl bromide to obtain the desired product. If the bromoacetyl bromide was added to a large excess of dry alcohol, a low-boiling product (b. p. 40° at 25 mm or 98° at 760 mm) was obtained instead of ethyl bromoacetate (b. p. 70° at 28 mm). No further characterization was attempted. The desired ethyl bromoacetate was obtained in 65% yield (based on bromoacetyl bromide) when the order of addition was inverted and the alcohol added to a stirred solution of bromoacetyl bromide. The reaction is very exothermic and better results were obtained when both reactants were diluted with dry benzene before the alcohol was added to the bromoacetyl bromide solution. Yields as high as 84% were obtained by using this procedure.

A four-step process was chosen to go from the ethyl bromoacetate to choline. First, the bromo group was displaced with dimethylamine to yield the ethyl ester of N, N-dimethylglycine. Second, the ester group was reduced with $LiAlH_4$ to yield the N, N-dimethylaminoethanol. Third, the amine was quaternized with methyl iodide to choline iodide. Fourth, the choline iodide was converted to the chloride on a column of the chloride form of Dowex 1- ×8 ion-exchange resin. This route was chosen over a displacement with trimethylamine, reduction, and ion-exchange to the chloride for the following reasons: First, there are literature references to the reduction of aminoacids to aminoalcohols with $LiAlH_4$,[35] and there are none to the reduction of betaine; furthermore, there are references showing a N-methyl migration when N-methyl quaternary compounds were treated with $LiAlH_4$.[36] Secondly, the chosen route allows a distillation step for purification just prior to the quaternization with methyl iodide. No important side reactions involving the amino alcohol would be expected in the quaternization step, therefore the distillation plus a couple of crystallizations of the choline as the bromide and then as the chloride should insure the purity and characterization of the product. A yield of 66% was achieved for the combined steps from the amino acid ester through the choline chloride.

The displacement of the Br atom by the dimethylamine was tried under a variety of conditions. Anhydrous reagents and nonpolar solvents were essential. When the reaction was run in alcohol or water a thick syrup resulted from which only dimethylammonium bromide could be crystallized. With toluene or benzene as the solvent,[37] up to 65% yields of the ethyl ester of N, N-dimethylglycine were achieved.

Route 3a in Table I indicates another route to the methyl ester of N, N-dimethylglycine. This thermal rearrangement of betaine was first described by Willstätter,[37] and yields up to 40% were achieved. Its usefulness is limited to deuteration of the 3-position with $LiAlD_4$. Since ethyl bromoacetate is available from Eastman Kodak Company, it is just as easy to make the ethyl ester of N, N-dimethyl glycine from ethyl bromoacetate and dimethylamine.

Routes 2, 3, and 4: Synthesis Procedures

Bromoacetyl bromide

A small amount (0.5 g) of acetic acid was distilled from 5.5 g of dry acetic acid to insure dryness. An initial 5 drops of PBr_3 was added and the cold N_2 stream and other temperature controls were adjusted, as shown in Fig. 4. Then dried Br_2 (dried over P_2O_5 and filtered) was added slowly, as the reaction proceeded, to avoid more than a light Br_2 color in the acetic acid. The reaction went to completion in about 4 hours. It was followed by collecting the evolved HBr in the dry-ice trap. The use of cold N_2 permits complete separation of the Br_2 and HBr. After this the flask was equipped with a vacuum distillation head and the excess bromine stripped out. After about 15 ml of benzoyl bromide was added, the product was distilled from 50° to 90° at 30 mm by using a 150° oil bath around the flask. The crude product was 12.9 g, giving an approximate yield of 85%. In general, intermediates were not purified and the yield figures are only approximate.

Ethyl bromoacetate

In a typical esterification, 2.73 ml of absolute alcohol was added to 10 ml of dry benzene. This was cooled to 0° and added to 9.65 g of bromoacetyl bromide in 15 ml of dry benzene. No HBr evolution occurred until the solution was refluxed. After refluxing of the solution for 1/2 hour the benzene was removed at 45° at approximately 200 mm. The product was distilled at 70° at 28 mm. The yield was 6.65 g, or 83% of the theoretical yield for this step. The over-all yield of ethyl bromoacetate, based on acetic acid-d_4, was 64.5%.

Condensation of dimethylamine and ethyl bromoacetate

After 8 ml of dry dimethylamine was distilled through a NaOH tube into a stoppered round-bottom flask at 0°, 25 ml of benzene at 6° was added. Then, after cooling to -78°, 10 g (6.6 ml) of 0° ethyl bromoacetate was added. A stopper was wired on and the solution allowed to warm to room temperature and sit overnight. It was important not to use less benzene and to be sure the benzene was frozen before adding the ethyl bromoacetate. Because this reaction is quite

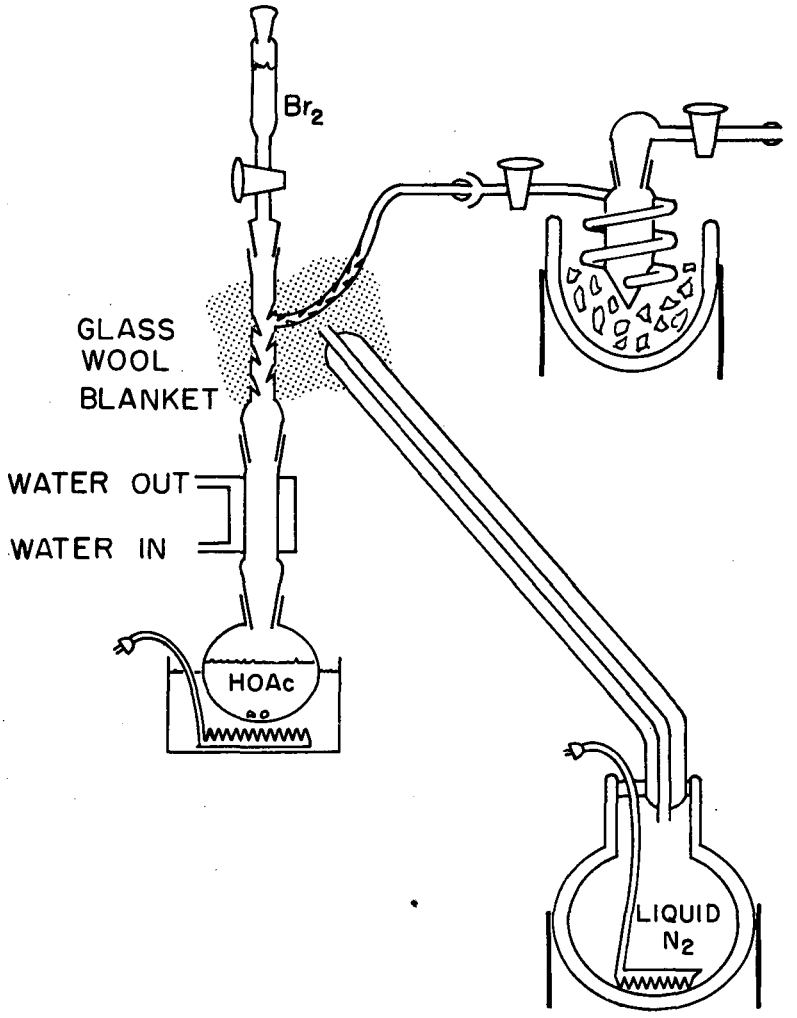

Fig. 4. Apparatus for the bromination of acetic acid.

exothermic, a large amount of frozen benzene was needed to control the dimethylamine pressure, both as a refrigerant before melting and as a solvent after melting. The sample was worked up by first distilling off most of the benzene and the excess amine. Then, after cooling to 7°, it was acidified to pH 2 to 3 and any unreacted ester was extracted into an ether phase. Next, aqueous phase was made alkaline with excess Na_2CO_3 and the aminoester extracted into an ether phase. After drying with Na_2SO_4 the product was distilled at 59°-62° at 30 mm. The yield was 5.0 g or 64% based on the bromoester.

The methyl ester of N, N-dimethylglycine from betaine hydrochloride

To make the free betaine, 40 g of technical betaine hydrochloride in 250 ml EtOH was stirred with 35 g of Ag_2O. After the AgCl was filtered off, 24 g or an 80% yield of free betaine was crystallized out. Seven grams of the free betaine was rearranged to the methyl ester of N, N-dimethylglycine by dry distillation from a 315° silicone oil bath. The 4 g of crude product was vacuum distilled to yield 2.82 g of the methyl ester of N, N-dimethylglycine (b. p. 49° at 27 mm). This was a 40% yield based on the free betaine.

Choline chloride from the reduction of the methyl ester of N, N-dimethylglycine

The crude ester of N, N-dimethylglycine from the thermal rearrangement of betaine was redistilled and 4.83 g of material boiling at 131°-135° at 760 mm was taken as the methyl ester of N, N-dimethylglycine. This was added to a solution of 814 mg of $LiAlD_4$ in 30 ml of dry ether (distilled off $LiAlH_4$). A considerable heat evolution occurred but virtually no gas was liberated. After the ether had refluxed 2 hours, it was decomposed by the careful addition of D_2O and extracted with ether. Since no D_2 evolution occurred the reaction mixture was slightly deficient in $LiAlD_4$. After addition of 3 ml of MeI to both ether and D_2O phases, 10 ml of alcohol was added to both phases and they were refluxed overnight. Finally, both fractions were vacuum evaporated to dryness and recrystallized with an ether–absolute-ethanol soltuion. The yield of deuterated choline iodide was 5.5 g, or 66% of the theoretical based on the aminoester. The sample was

converted to the choline chloride on a Dowex-1 column and recrystallized after Nuchar treatment. The yield of choline chloride-d_2 was 1.091 g, or 90% based on the crude choline iodide.

C and H Analysis and NMR as Characterizations of Deuterated Choline Chlorides

It is not possible to characterize choline chloride and its deuterated analogs by melting points. These quarternary ammonium salts all start to decompose with gas evolution at 180°-200° before there is any indication of melting. The formation of derivatives is a useful way to check the presence of functional groups; however, it is not useful for determining purity as it can give rise to fractionation. For these reasons the characterization of the deuterated cholines was done by C and H analyses and NMR spectroscopy. The C and H analyses proved useful for identifying side-reaction products such as $(Me)_2\overset{+}{N}H_2\ Br^-$. This is the only material recoverable when the condensation of dimethylamine and ethyl bromoacetate is run in alcohol and the $(Me)_2\overset{+}{N}H_2\ Br^-$ precipitates in pure crystals. If, however, one has a small percentage of compounds similar to the desired product that coprecipitate with it, then the C and H analysis is not a useful method for determining purity.

Nuclear magnetic resonance (NMR) provides a useful analytical tool for characterizing choline chloride. Since the hydrogen nucleus has a magnetic moment and spin moment, it, like the unpaired electron, exhibits a spin-resonance phenomenon. Since the magnetic moment is much smaller, the resonance occurs in the radiofrequency region. For a proton resonance at 40 Mc one needs a field of about 3.58 kilogauss. The extremely weak interactions of the nuclei with their environment gives rise to line widths of only a fraction of a milligauss. It is this extremely narrow line width that makes it possible to observe the diamagnetic shielding effects of the near-by paired electrons, usually referred to as the "chemical shift" (δ), and the hyperfine interaction between protons. Although some homologous series, and other special cases, show extrapolatable values of the chemical shift, generally speaking the NMR spectra are measured but not predicted.

NMR spectra of 30% solutions of choline chloride and its analogs in D_2O are shown in Fig. 5. The proton position that has been deuterium-substituted is indicated by the formulas. The pure, undeuterated choline chloride solution shows a considerable hyperfine interaction between the methylene protons which broadens and splits their spectra. Spectrum 1 is exactly as expected with the N-methyl proton spectrum gone. Spectrum 2 is likewise missing the N-methylene proton spectrum and the N-methylene line is much sharper as a consequence of the elimination of the proton hyperfine interaction of the methylene groups. It is much sharper than the O-methylene. This suggests that the N-methylene has less of a barrier to rotation than the O-methylene. Spectrum 3 is similar to 2 only with the O-methylene proton spectrum missing. Here, however, the O-methylene is not as sharp a line as the NCH_2 is in spectrum 3, and suggests a doublet. This may arise from restricted rotation of this methylene group. In no case is there any serious evidence of impurities. The C and H analyses in Table II are considered quite satisfactory for a compound as deliquescent as choline chloride. The spectrum and C and H analysis of the impure second crop of crystals of 2-deutero choline chloride are particularly noteworthy. No impurities would be suspected from the C and H analysis but the NMR spectrum clearly shows the presence of sizable amounts of impurities. The small arrows point to the extra peaks. A possible impurity is shown in Table II. This is consistent with both the NMR and C and H analysis data, but is strictly hypothetical as it has not been isolated. It could easily arise from a methylamine impurity in the dimethylamine.

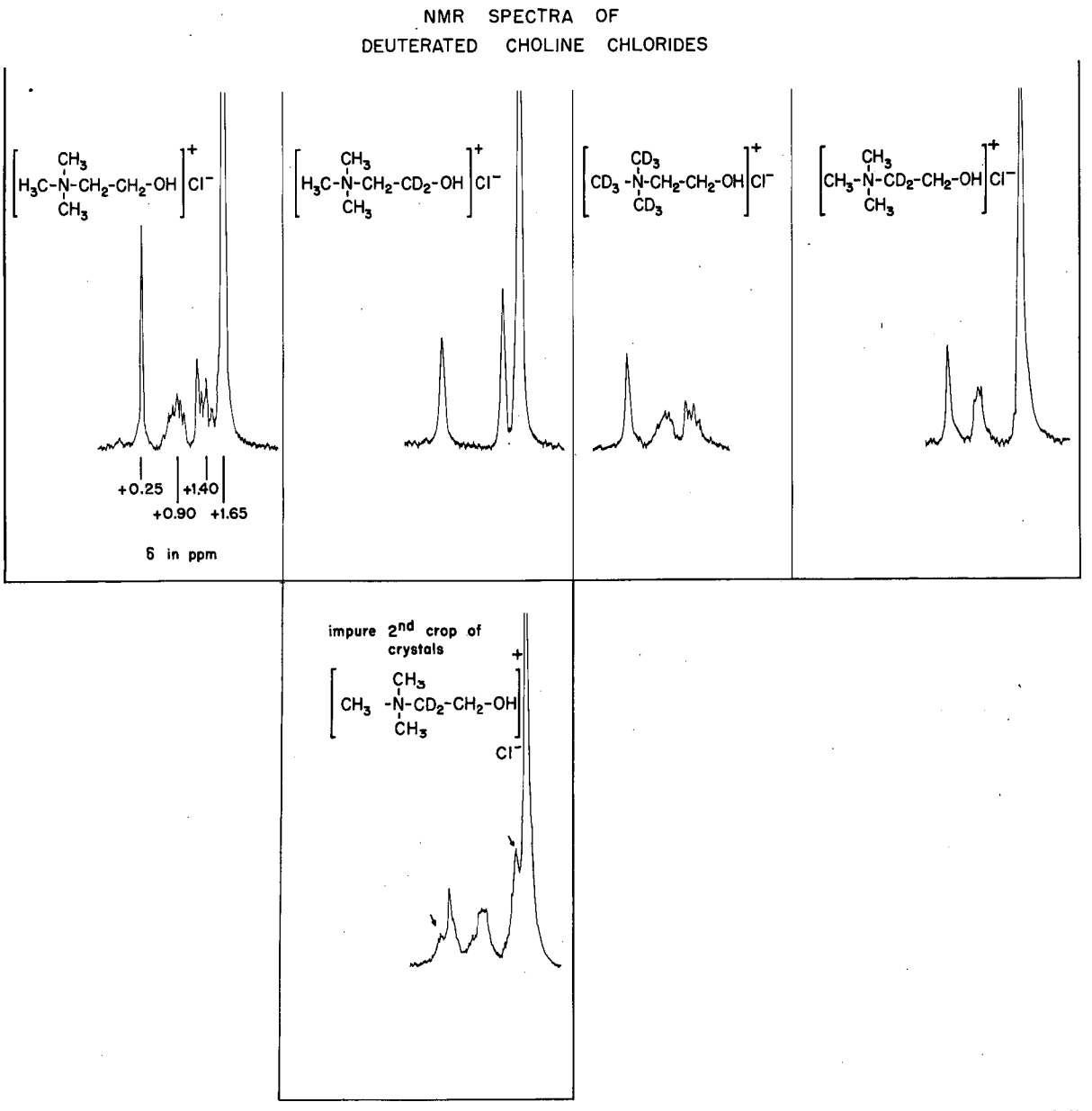

Fig. 5. NMR spectra of deuterated choline chlorides.

RADICAL CHARACTERIZATION WITH ELECTRON-SPIN RESONANCE SPECTROSCOPY

Introduction to Electron-Spin Resonance

Although electron-spin resonance spectroscopy was originally developed by physicists[38] and used on inorganic systems, its uses have grown and expanded very rapidly into the study of organic radicals. In many cases it yields detailed information about radical structure, and in nearly every case relatively accurate measurements of radical concentrations greater than 10^{-5} M are possible. For these reasons electron-spin resonance (ESR) spectroscopy is one of the most valuable tools now available to the chemist and physicist for measurements on unpaired electrons.

Electron-spin resonance is a consequence of the angular momentum and magnetic moment possessed by electrons. In a static magnetic field (H_0) the magnetic moment of the electron is quantized and has two allowed orientations: with and against H_0. Hence, there exist two states differing in energy by $2\,\mu H_0$, where μ is the effective magnetic moment of the electron. This is a quantized system and, as a consequence, only integral changes in the values of the energy of the system and of the angular momentum are allowed. The situation is quite analogous to the electronic energy levels in an atom. It differs in that the energy levels of an atom are fixed by the number of occupied levels, where the difference in the energy levels of the electron spin system is proportional to H_0. When electromagnetic quanta with the correct polarization and size interact with the electron, transitions are induced. At thermal equilibrium these two states are not equally populated but rather have a distribution determined by the Maxwell-Boltzmann distribution law. At thermal equilibrium the lower state has a slight excess in population over the upper. Since the probability of a transition is the same for an electron in either state, the net result is a greater number of transitions up than down; that is, absorption of power occurs. The criterion for absorption is that the quantum size be equal to the difference in energy levels of the spin states. This is usually given as $Hv = g\,\beta\,H_0$,

H = Planck's constant,

ν = the microwave signal frequency,

g = spectroscopic splitting factor,

β = the Bohr magneton,

H_0 = the static magnetic field.

This is illustrated with the dotted-line portion of Fig. 6. Formulation in this way with a spectroscopic splitting factor allows the easy inclusion of those cases in which the orbital magnetic moment is not completely quenched and it contributes to the energy of the spin state. Important contributions are found for ions of the transition and rare earth groups, but organic radicals show little orbital coupling. Practically all the published g values are within 0.2% of the free-electron value of 2.0023.

Nuclear Hyperfine Interactions

Many nuclei, like the electron, possess angular momentum and a magnetic moment and show resonant absorption. Although this work is primarily concerned with hydrogen and deuterium interactions with electrons, in Table III data on a number of other species are included for comparison and to indicate those systems in which isotopic substitution might prove useful in ESR data. Nuclear magnetic resonance as such was used for isotopic analysis and is discussed in the section on synthesis. In this section on ESR the nuclear hyperfine splitting of the unpaired-electron absorption is discussed. The simplest possible case is represented in Fig. 6, where the splitting of a free-electron absorption and its energy levels (depicted with broken lines) by a hydrogen nucleus into a new set of lines is shown. In the case in which the unpaired electron spends all its time on one hydrogen (i. e., atomic hydrogen) a doublet with a hyperfine splitting of 505 gauss is expected--and has been observed by Livingston, Zeldes, and Taylor.[39] These authors observed this species in irradiated acids at low temperatures. This type of situation, in which a radical species is unambiguously characterized by the type and size of a hyperfine spectrum is relatively rare. Some more general situations than a single-proton interaction are the following. First, if a single nucleon with a spin of M_i interacts

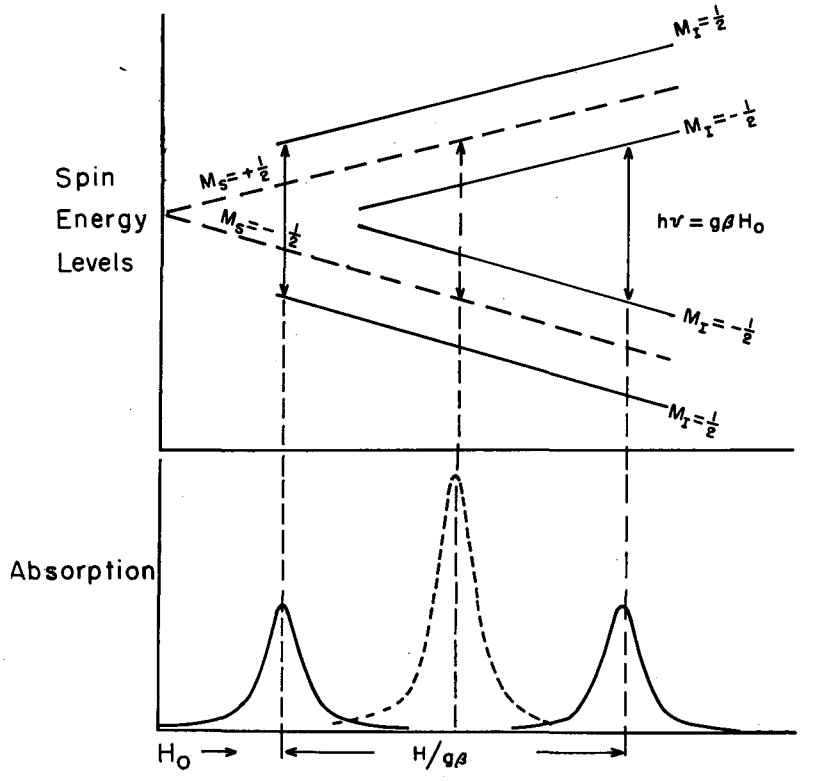

MU-17659

Fig. 6. This figure illustrates in the broken lines the energy levels and ESR spectrum of an electron. The solid lines illustrate the result of a weak hyperfine interaction with a proton.

Table III

Spin moments of interest in connection with nuclear hyperfine splitting of unpaired electrons

Species	Natural abundance	Magnetic moment, $u = \frac{eh}{MC}$ (nm)	Spin moment (h)
e	--	-1836.	1/2
H^1	99.98	2.79	1/2
H^2	$1.56\ 10^{-2}$	0.857	1
C^{12}	98.89	0.00	0
C^{13}	1.11	0.70	1/2
N^{14}	99.6	0.403	1
N^{15}	0.365	-0.283	1/2
O^{16}	99.75	0.00	0
O^{17}	$3.7\ 10^{-2}$	-1.893	5/2
O^{18}	0.20	0.00	0
S^{32}	95.1	0.00	0
S^{33}	0.74	0.6279	3/2
S^{34}	4.2	0.00	0

with an electron, then $2M_i+1$ lines result. Disodium peroxylamine disulfonate is an example with $M_i=1$, therefore three equal-intensity lines are expected, and they are found.[40] Secondly, for n protons this gives rise to a maximum of 2^n equal-intensity lines. However, fewer lines result when the same spin energy level arises from more than one spin state. Thus, two nonequivalent protons give rise to four lines, but if they are equivalent then the two states with opposing spins merge to a doubly degenerate state and three lines with a 1:2:1 intensity distribution are found. For n equivalent protons this gives rise to n+1 lines whose intensities follow the binomial coefficients in $(a+b)^n$. (For example, n=0, 1, 2, 3, 4 gives intensity distributions of 1, 1:1, 1:2:1, 1:3:3:1, 1:4:6:4:1). A number of the simpler cases embracing these situations are tabulated in Table IV. In terms of spectra, the relative intensities of the lines are given by D, the degeneracy of each hyperfine energy level. The hyperfine energy levels or amounts of splitting of the electron spin spectra are specified by ΣA_i, where A_i is the contact term of the ith-proton hyperfine interaction; ΣI_i is the net spin of each spin state.

Examples in which the hyperfine interaction constants have multiple relationships to one another obviously typify only the completely degenerate cases in which no amount of resolution can separate the overlapping lines. In practice, a range of values of interaction constants rather than a single value will give an observed spectrum of the same general appearance. The effect of small differences in the values of the proton hyperfine interactions is to broaden the individual lines and thus reduce the effective resolution. Thus the line width and resolution are important along with the number and type of hyperfine interactions in determining the observed nuclear hyperfine spectrum. The amount of isotropic hyperfine splitting is a measure of the unpaired electron concentration at the nucleus producing the splitting. Thus the amount of splitting produced by different nuclei can be used to measure the unpaired-electron distribution within a radical species.

Table IV

Case	Interacting Species No.	Type	Interaction constants	Models for spin energy levels	Degeneracy	Spin moment I_n	Spin energy level A
A	2	H^+	1,1	↑↑	1	1	2
				↑↓ ↓↑	2	0	0
				↓↓	1	-1	-2
B	2	H^+	2,1	↑↑	1	1	3
				↑↓	1	0	1
				↓↑	1	0	-1
				↓↓	1	-1	-3
C	3	H^+	1,1,1	↑↑↑	1	3/2	3
				↑↑↓ ↑↓↑ ↓↑↑	3	1/2	1
				↓↓↑ ↓↑↓ ↑↓↓	3	-1/2	-1
				↓↓↓	1	-3/2	-3
D	3	H^+	1,1,2	↑↑↑	1	3/2	4
				↑↑↑ ↑↓↑	2	1/2	2
				↑↑↑ ↑↓↓	2	±1/2	0
				↑↓↓ ↓↑↓	2	-1/2	-2
				↓↓↑	1	-3/2	-4

Table IV (cont.)

Case	Interacting Species No.	Type	Interaction constants	Models for spin energy levels	Degeneracy	Spin moment I_n	Spin energy level A
E	3	H^+	1,2,2		1	3/2	5
					1	1/2	3
					2	1/2	1
					2	-1/2	-1
					1	-1/2	-3
					1	-3/2	-5
F	3	H^+	1,2,3		1	3/2	6
					1	1/2	4
					1	1/2	2
					2	1/2, -1/2	0
					1	-1/2	-2
					1	-1/2	-4
					1	-3/2	-6

Table IV (cont.)

Case	Interacting Species No.	Type	Interaction constants	Models for spin energy levels	Degeneracy	Spin moment I_n	Spin energy level A
G	3	H^+	1,2,4		1	3/2	7
					1	1/2	5
					1	1/2	3
					1	-1/2	1
					1	1/2	-1
					1	-1/2	-3
					1	-1/2	-5
					1	-3/2	-7
H	4	H^+	1,1,1,1	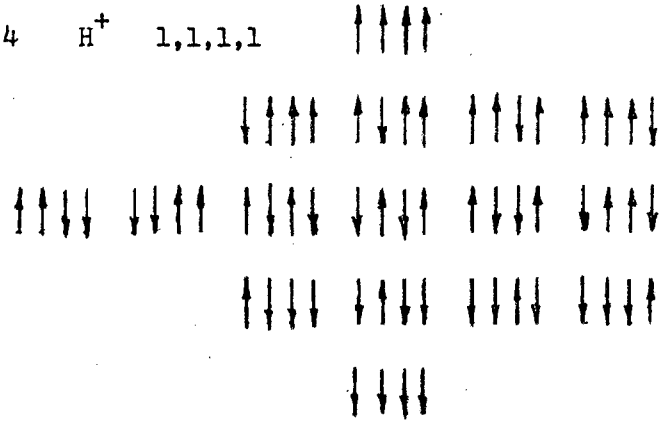	1	2	4
					4	1	2
					6	0	0
					4	-1	-2
					1	-2	-4

Table IV(cont.)

Case	Interacting Species No. Type	Interaction constants	Models for spin energy levels	Degeneracy	Spin moment I_n	Spin energy level A
I	$N+H^+$	1,2		1	3/2	3
				1	1/2	2
				1	-1/2	1
				1	1/2	-1
				1	-1/2	-2
				1	-3/2	-3
J	$N+H^+$	1,1	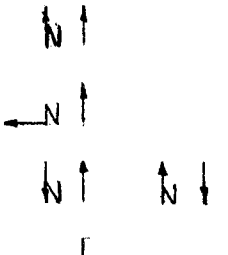	1	3/2	2
				1	1/2	1
				2	-1/2, 1/2	0
				1	-1/2	-1
				1	-3/2	-2
K	$N+H^+$	2,1	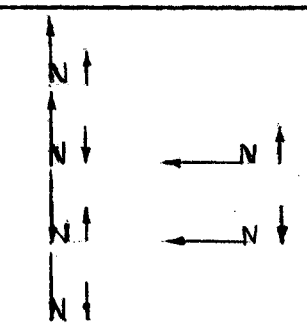	1	3/2	3
				2	1/2	1
				2	-1/2	-1
				1	-3/2	-3

Table IV (cont.)

Case	Interacting Species No. Type	Interaction constants	Models for spin energy levels	Degeneracy	Spin moment I_n	Spin energy level A
L	N,H^+,H^+	2,1,1		1	2	4
			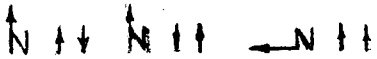	3	1	2
			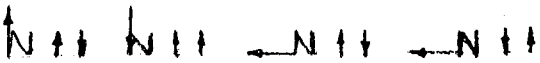	4	0	0
				3	-1	-2
				1	-2	-4
M	N,H^+,H^+	2,2,1		1	2	5
				2	1	3
				3	1,0,0	1
				3	-1,0,0	-1
				2	-1	-3
				1	-2	-5

A large number of tentative radical assignments have been made on the basis of the number of hyperfine absorption lines and their intensity distribution. There is usually chemical information available on the structure of the starting material and on the products, which must both be consistent with the ESR hyperfine information. For aromatic structures simple molecular orbital theory can be taken as a tentative guide to the relative stability of different hypothetical radical intermediates. Considerable literature exists in which these ideas have been used and shown to apply fairly well. Wertz and Vivo[41] have examined the radical intermediates produced in the alkaline reduction of the unchlorinated, mono-, di-, tri-, and tetrachloroquinones. The expected n+1 proton hyperfine lines were observed and the intensities were approximately binomial except for the trichloro compound. This nonconformity may have been due to an impurity. Although a few relatively stable radicals such as diphenylpicrylhydrazyl are well known, most radicals are reactive and unstable. As a consequence, in most reactions it is difficult to be certain that the spectrum is for only one radical species and not a composite of several superimposed radical spectra. The problem is even worse if, as frequently happens, the spectrum is not completely resolved, so that the intensity distribution is nearly indeterminate. In these circumstances, and particularly if the chemistry is not well known, the radical structural assignments become increasingly more tentative, and confirmation by isotopic substitution becomes desirable.[42] ESR is finding frequent application in the study of radicals produced by irradiations. It has been used to study the radicals produced in polymers by radiation,[43] and also to study radical intermediates in polymerizing vinyl monomers.[44] Ingram has been using it to study some photochemical reactions of alcohols and peroxides in a frozen matrix. Although several authors[21, 17, 45, 46] have studied the radicals produced by a variety of high-energy radiation sources (from 50-kev x-rays to 2-Mev e^-) in amorphous organic solids at low temperature, only a very few examples can be found in which the irradiation study was thorough enough to reveal much of the radiation chemistry. There has been a tendency to draw conclusions that go beyond the data on which they are based.

Unless there is a body of previous chemical experience to act as a guide, using only the ESR hyperfine spectra of protons can be misleading. In his early paper Gordy[45] speculated on $(CH_2)^+$ as the radical species produced from irradiated methanol. Alger, Anderson, and Webb[17] have pointed out that the production of ethylene glycol, which has been reported by McDonnell and Newton,[47] is good evidence for $\cdot CH_2OH$ as the intermediate radical, although the two experiments are not strictly comparable. This leaves the unanswered question of why the hydrogen on the oxygen does not cause an observable hyperfine interaction. ESR studies on irradiated polycrystalline solids and biological materials have been made by Gordy[48, 49] and his associates. The emphasis in most of the examples cited has been the characterization of organic radicals with proton hyperfine ESR spectra. The hyperfine interaction can be looked on as the sum of two components:[50] an anisotropic term, which results from direct dipole-dipole interaction of the unpaired electron and the perturbing nuclei, and an isotropic term--the Fermi contact term--which is proportional to the unpaired electron concentration at the perturbing nucleus. Studies of dilute single crystals are potentially the most informative system for ESR work, since they not only give more highly resolved spectra but the position of the anisotropic terms can be shifted by changing the orientation of the crystal in the magnetic field. Radicals in solution also can give excellent resolution if the molecules are free to tumble at a frequency that is high compared with the anisotropic hyperfine splitting. Radicals frozen in an amorphous matrix usually are not free to tumber and hence show the anisotropic portion of their spectra as smeared-out spectra underlying the isotropic portion. Radicals in a polycrystalline system are at best similar to the amorphous matrix. However, they sometimes show structure suggesting that the crystals are somewhat oriented and some weak anisotropic hyperfine lines are starting to appear.

Most frequently ESR is a tool to study a chemical system, and the system determines the form of the material used. Irradiated choline chloride is a case in point. Since the unusual aspect of its

radiation damage (i. e., the large G value) occurs only in crystalline samples, solution studies would show nothing at all, and studies in an amorphous matrix would not have any obvious relationship to the radiation damage in crystals. This leaves the single-crystal and polycrystalline systems to be considered. The radicals generated in choline chloride by irradiation have a relatively short half life of a few hours. Furthermore, choline is deliquescent and the crystals dissolve in their own absorbed water when they are exposed to air for a few minutes. This indicates the need to enclose the choline chloride in a glass tube to protect it from moisture during the irradiation and ESR observation. F centers are formed in the glass sample holder during irradiation and interfere with observation of the ESR spectrum of the sample. The procedure used to avoid this difficulty was to irradiate only one end of the sample tube with a linear accerlerator and then to invert the tube and slide the sample to the nonirradiated end for ESR observation. However, this procedure was not easily adapted to single-crystal work, where alignment of the crystal in the magnetic field (H_0) is necessary. Consequently, almost all the samples whose spectra were taken were polycrystalline. Choline chloride crystallizes as long orthorhombic needles. When it was rotated with its longitudinal axis perpendicular to H_0 only very minor shifts in the spectrum were observed. Since then, other workers[51] have observed the spectral changes when single crystals were rotated about their transverse axes, with the axis of rotation perpendicular to the field H_0. When the longitudinal axis was perpendicular to H_0 the spectrum was very similar to that of a polycrystalline sample. The only apparent difference was a slightly improved resolution. When the longitudinal axis was parallel to the field, a complex and only partially resolved thirteen-line spectrum appeared.

ESR Experimental Procedures

All the ESR spectra were determined on equipment designed and built by Dr. Power B. Sogo at the laboratories of the Bio-Organic Chemistry Group of the Lawrence Radiation Laboratory. This equipment is called a derivative ESR spectrometer, as its output approximates a derivative of the ESR absorption spectrum. A block diagram of the ESR spectrometer is shown in Fig. 13.(in the section on Standards). The output frequency of the klystron is locked to the cavity resonant frequency with a standard automatic-frequency-control loop from the output side of the cavity to the klystron reflector circuit. The cavity operates in a H_{011} mode at 9.3 kilomegacycles. In spite of openings at the top and bottom for sample insertion it has a Q of approximately 10,000. The electromagnet current supply incorporates a regulator and is swept with a linear sweep from either a clock motor and helipot, or a triangular sweep generator. The microwave system is normally run at about 4 milliwatts. The microwave signal is detected with a set of matched bolometers in a dc bridge circuit that responds to the modulation envelope of the microwave field. This modulation is a consequence of the modulation of the ESR absorption, which varies instantaneously with the audio modulation of the static magnetic field. The modulation circuit operates at a frequency of about 200 cycles and is adjusted so that the amplitude of the magnetic field sweep is somewhat less than one-half the line width of the spectrum under observation. This is a compromise, as better resolution is available with smaller modulation amplitudes. However, this smaller amplitude also reduces the sensitivity.

Two benefits derive from this type of spectrometer. First, it gives a much better signal-to-noise ratio than a direct absorption measurement. Second, the shape of the signal observed is approximately a derivative of the ESR absorption signal shape. This is of significant help in the interpretation of partially resolved hyperfine structure, as the interpretable changes in slope are much more emphatic than the corresponding changes in shape of an absorption curve.

The treatment of these derivatives with a double-integral or first-moment procedure to get the integrated ESR absorption is justified in the section on ESR standards. The preparation and irradiation of the samples before their ESR spectra are taken is described in the sections on synthesis and irradiation.

All the ESR spectra were determined at room temperature after preliminary work showed the resolution at -170° was poorer than that obtainable at room temperature. This is an indication that the line width is due to unresolved hydrogen or nitrogen hyperfine coupling to near-by nuclei rather than spin-lattice interaction. Reducing the temperature would decrease spin-lattice interaction and reduce line width controlled by this interaction. That this narrowing is not observed shows this interaction is not important. The observed increase in line width, shown by a reduction in resolution, indicates that at 20° we already have important motional narrowing of the spectra. Unfortunately, higher temperatures accelerate the rate of disappearance of the radicals, and therefore have not been used.

ESR Measurements on Irradiated Compounds

In the initial stages of the choline chloride irradiation program a number of compounds with structural similarities were irradiated and examined with the ESR equipment. It was expected that some correlations would be observed between the structure and the spectrum. These spectra are shown in Figs. 7 through 11. They are only qualitative, and although the samples were finely divided powders, crystal field effects were readily apparent on rotation of the samples. The curved appearance of some of the spectra is a consequence of recording them with an Esterline-Angus recording galvanometer. Although in the NH_4Cl the radicals decayed too rapidly for observation at room temperature, a number of other cases showed virtually no decay over a 3-month period at room temperature. In nearly every case better resolution could be found at room temperature than at -170°. Observations on some of the samples are contained in Table V. The loss of hyperfine structure by choline chloride on cooling from room temperature (Fig. 6-1) to -170° (Fig. 6-2) is very striking, and its

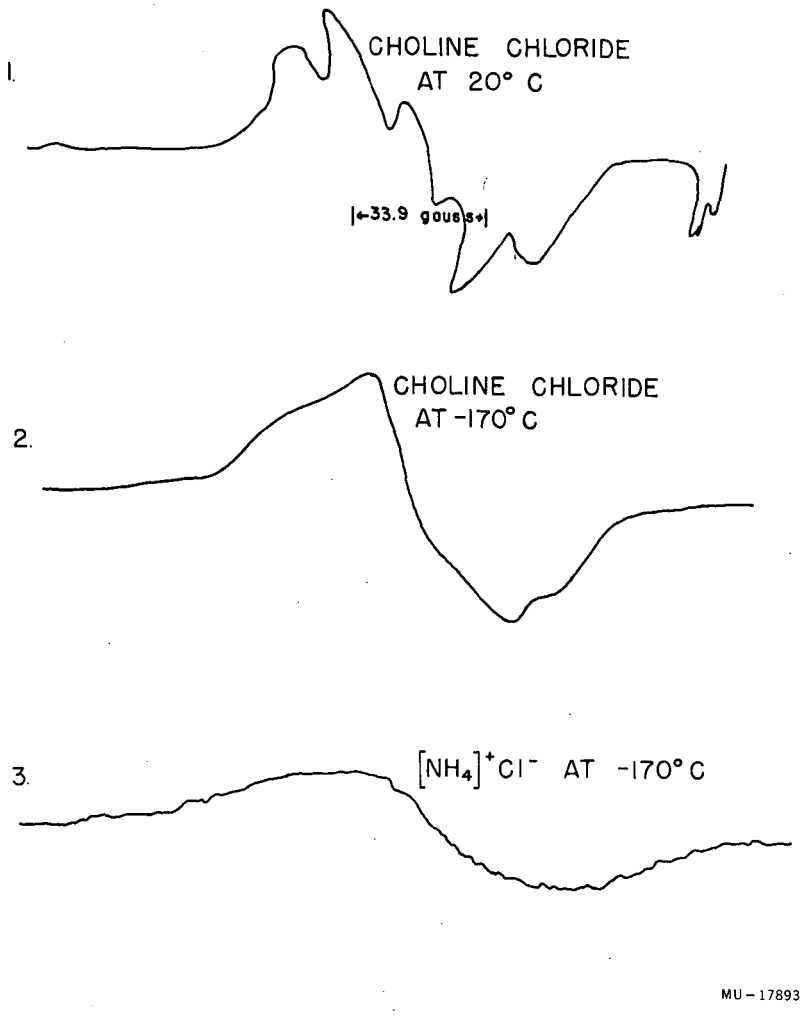

Fig. 7. ESR spectra of irradiated choline chloride and related compounds.

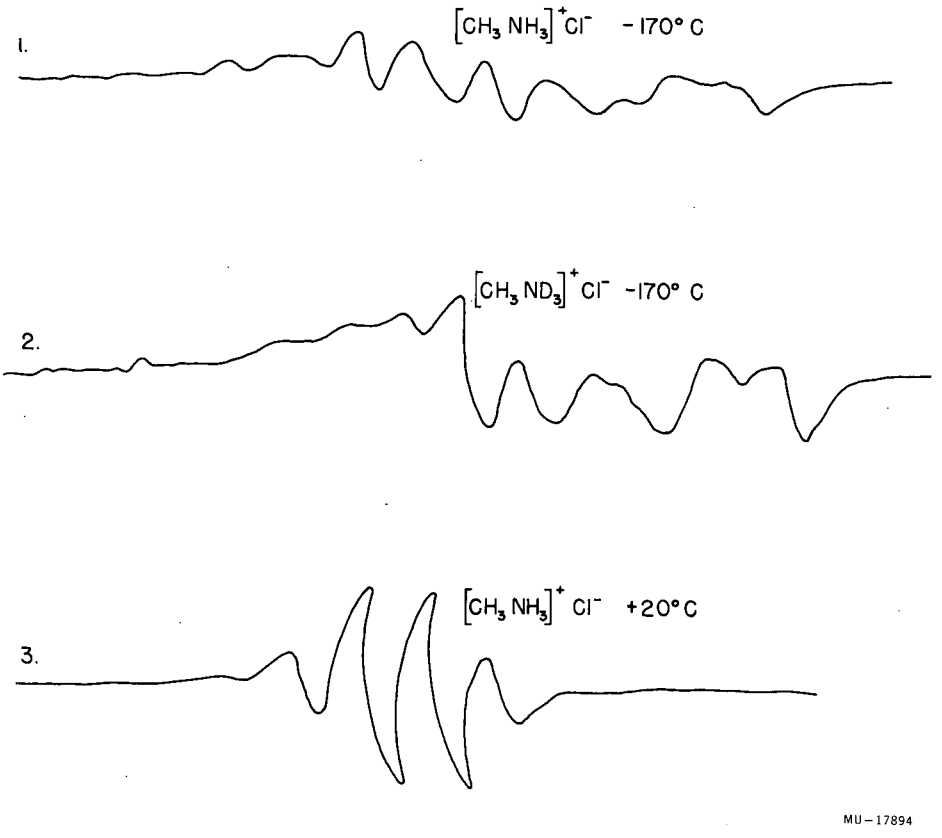

Fig. 8. ESR spectra of irradiated analogs of choline chlroide.

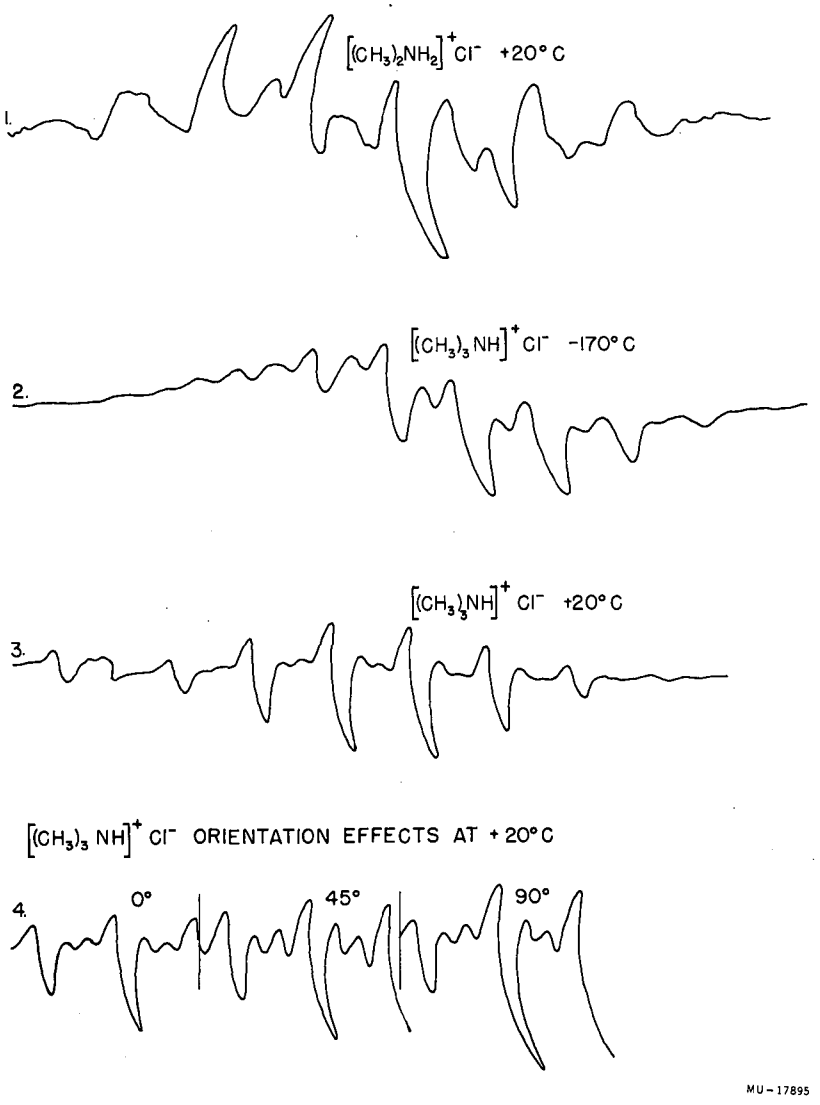

Fig. 9. ESR spectra of irradiated analogs of choline chloride.

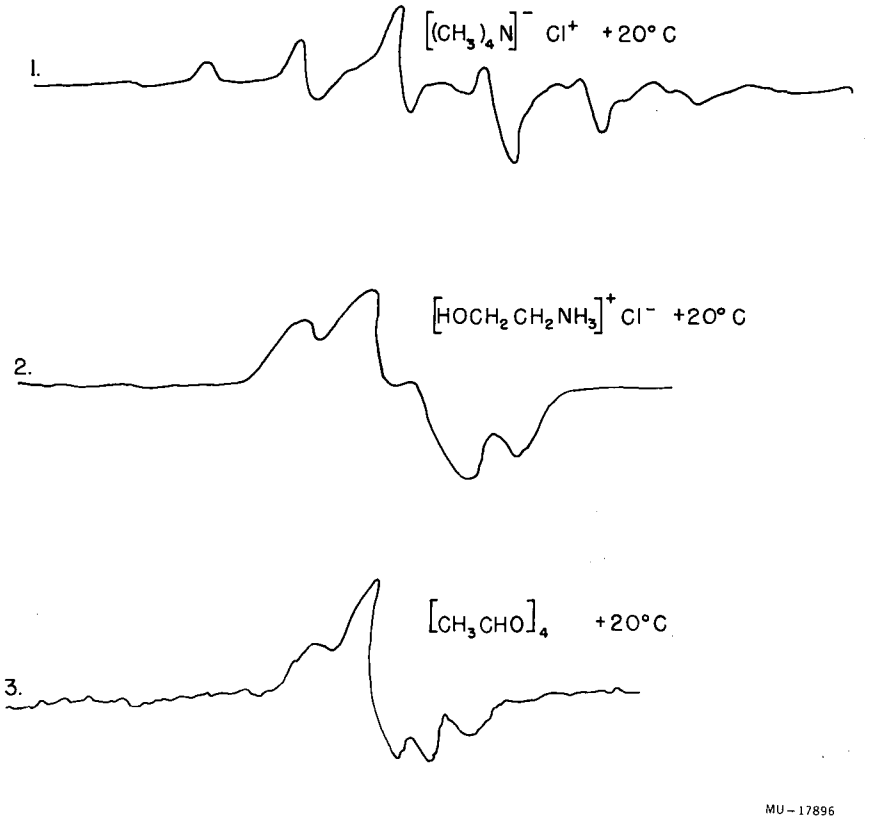

Fig. 10. ESR spectra of irradiated analogs of choline chloride.

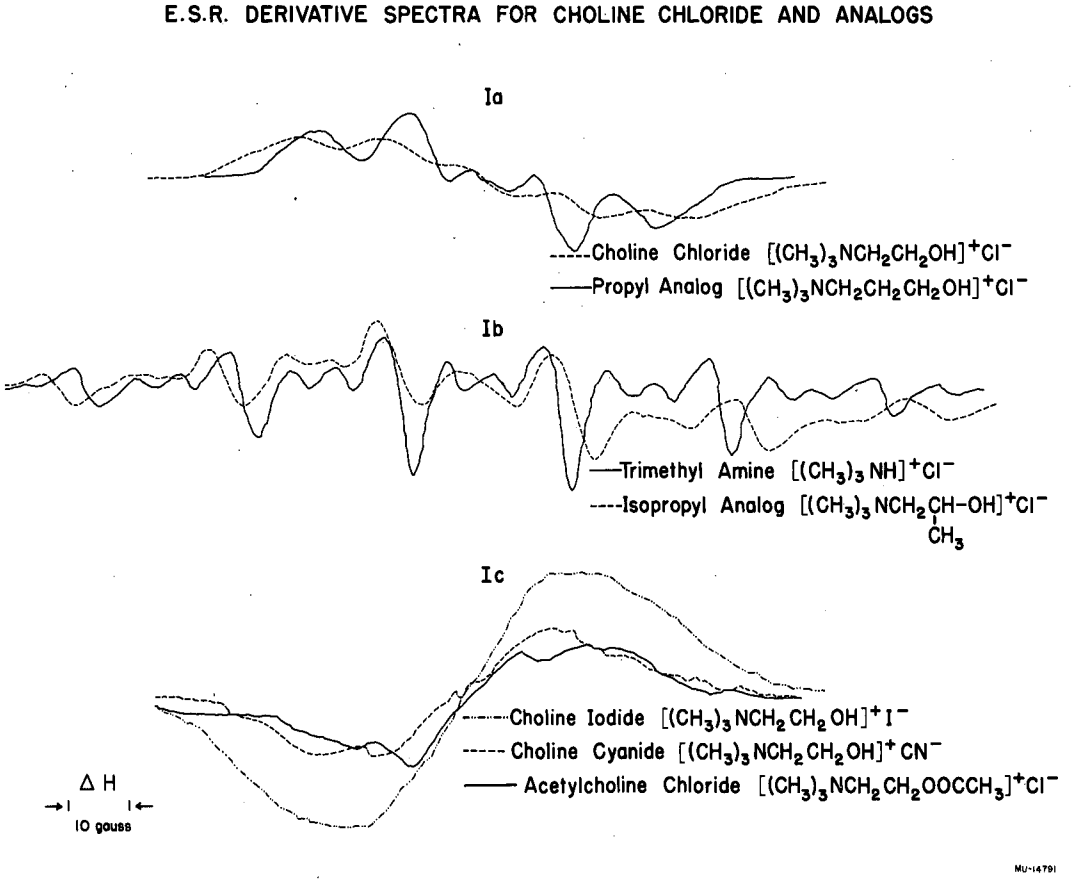

Fig. 11. ESR spectra of irradiated choline chloride and some analogs.

Table V

Relative radical stability of some irradiated choline chloride analogs

Radiation dose: 7.45 megarads of 4.5-Mev e^- at -170°C

Sample	Color after irradiation	Relative signal	Comments
$[NH_4]^+Cl^-$	yellow	0	Radical and color decay too rapidly to observe at room temperature
$[CH_3NH_3]^+Cl^-$	white	1	Radicals decayed to 1/4 in 4 hours
$[(CH_3)_2NH_2]^+Cl^-$	yellow	1/2	Decayed to 1/4 in 5 hours
$[(CH_3)_3NH]^+Cl^-$	orange	1	Radicals stable over a 3-month period
$[(CH_3)_4N]^+Cl^-$	yellow	1	Radicals stable over 3-month period
$[HOCH_2CH_2NH_3]^+Cl^-$	white	2 1/2	Radicals decay to 1/2 in 3 hours
$[CH_3CHO]_4$	white	1/2	Radicals decay to 1/2 in 3 hours

interpretation as motional narrowing has already been discussed. Choline chloride has an approximate hyperfine intensity ratio, indicated by peak-to-peak heights of the derivative curve, of 1:3:3:3:1. Depending on the orientation of the sample, other intensity ratios varying down to 1:2:2:2:1 have been observed. This is attributed to contributions from anisotropic components as a result of incompletely randomized orientation of the crystalline powder.

On the basis of the original work (Fig. 7) the radical spectrum was tentatively assigned to a proton hyperfine interaction of the type shown in Case D in Table IV, in which the electron interacts equally with either of two protons and twice as strongly with a third proton. Later work with deuterium indicated Case H, with four equivalent protons, as a better assignment. Radical assignments for this case are discussed in the section on deuterated choline chlorides.

The spectrum of irradiated NH_4Cl (Fig. 7-3) is uninformative, since it shows no hyperfine structure at -170° and decays too rapidly to permit observation at room temperature. The spectrum of methylamine hydrochloride (Fig. 8-1) is interesting because it shows more and different spectra at -170° than at room temperature. This structure is probably due to several radicals with different decay rates, since, after warming, only one spectrum of four lines in a 1:3:3:1 ratio remains. This is the spectrum that would be expected from three equivalent protons interacting with an unpaired electron, as is depicted in Table IV, Case C. In irradiated methylamine hydrochloride, this can be best assigned to trapped methyl radicals. The irradiated di-, tri-, and tetramethyl ammonium chlorides (Figs. 9 and 10) showed much more dependence of their spectra on the sample orientation and have more complex spectra. The spectra were so obviously different from those of choline chloride that very little work was done with them. The irradiated tri- and tetramethyl ammonium chlorides should be amenable to single-crystal studies, since both show very slow radical decay rates.

Irradiated ethanol ammonium chloride (Fig. 10-2) shows a spectrum with some general similarities to that of irradiated choline

chloride. The intensity distributions in this spectrum are about 1:3:3:1, therefore it can be assigned to electron interaction with three equivalent protons (Table IV-C). Because of the similarity of the spectra to that of choline chloride, the radical assignment is discussed in the section on deuterated choline chlorides. The metaldehyde (Fig. 10-3) gave a very asymmetrical spectrum and no radical assignments were attempted.

The ESR derivative spectra of some irradiated choline chloride analogs and choline chloride are shown in Fig. 11. The spectra of choline iodide, choline cyanide, and acetylcholine chloride (Fig. 11-1c) are so poorly resolved that no useful hyperfine splitting can be discerned. It is not possible without further work to decide whether this lack of hyperfine structure is due to a change in radical structure via a radical transfer reaction, or to a change in the structure of the crystal cage in which the radical is contained. The latter could occur in a number of ways. A change in crystal structure that restricts the rotation of the radical would reduce motional narrowing and broaden the lines. Any change in crystal structure that puts the protons or nitrogen of the neighboring molecules closer to the unpaired electron causes broadening of the absorption lines. The hyperfine spectra of irradiated trimethylamine hydrochloride, of the chloride salt of choline, of the chloride salt of the propyl analog, and of the chloride salt of the isopropyl analog are somewhat more informative.

For choline chloride, the five-line spectrum appears to have a 1:3:3:3:1 intensity distribution. The poor resolution makes it difficult to be certain of the actual line intensities. This is discussed in the next section.

The propyl-analog spectrum superficially resembles that of choline. However, the intensities are very different and spectra without the weak central lines have been observed, so that this may be attributed either to a weak anisotropic line or to another radical. It appears best to treat this spectrum as a four-line spectrum with a 1:2:2:1 intensity distribution and with a weak singlet of some other radical in the center. This 1:2:2:1 intensity distribution can arise from a single radical with the nitrogen and proton orbitals such that

the unpaired electron distribution results in twice as much interaction with the N nucleus as with the proton, and is illustrated in Table IV, Case K. The broad underlying spectrum, lack of resolution between lines, and apparent interference from weak spectral lines arising from other radicals make such an assignment quite tentative. The uncertainty attendant upon the intensity measurements makes it useful to consider other intensity ratios, such as 1:3:3:1, which also might give rise to the observed spectrum. This type of hyperfine distribution arises from an electron interacting equally with three equivalent protons. This is illustrated in Table IV, Case C. Determining the spectra of selectively deuterated and N^{15} analogs would certainly allow the assignment to be unambiguously resolved. Single-crystal studies should also be practical as a consequence of the long life of the radicals (radicals decayed to 1/10 in 20 days). It is quite possible that single-crystal work would show spectra with sufficiently sharp lines to allow an unambiguous assignment of the radical structure.

The spectra of the irradiated isopropyl analog of choline chloride and of trimethylamine hydrochloride are shown together because of the similarities in their spectra. It is reasonable to assign the weak recurring absorptions to anisotropic components, since their relative amplitudes depend on the orientation of the sample in the static magnetic field, H_0. The intensity ratios observed for the strong lines are 1:2:3:3:2:1. A situation that can give rise to this type of spectrum is shown in Table IV, Case M. It requires interactions by the unpaired electrons with a N and two protons. The relative strengths of the interactions need to be as two for the nitrogen, two for the first proton, and one for the second proton. Since the trimethylamine part of the molecule is the only part common to these two molecules, the similar spectral features suggest that the radical structure is centered in this portion of the molecule.

ESR Measurements on Deuterated Choline Chlorides

In Fig. 12 are shown the ESR spectra of irradiated samples of choline chloride and its deuterated analogs. Of the deuterated compounds, only those selectively deuterated in the 1 (N-methyl), 2 (N-methylene), and 3 (O-methylene) positions have their spectra shown in Fig. 12. (The compound deuterated in the O-D position was also run; its spectrum indistinguishable from that of the undeuterated sample, was omitted from Fig. 12.) The spectrum of the 1-deuterated compound has nearly all the same spectral features as the undeuterated spectrum, but differs in having a slightly better resolution. This indicates that part of the observed line width of the undeuterated sample is due to unresolved hyperfine structure caused by weak interactions by the nine protons in the 1 position with the unpaired electron. This is also consistent with the earlier observation that the decrease in resolution with reduced temperature resulted from unresolved hyperfine structure with motional narrowing. The apparent loss of resolution in the spectra of the 3-deutero compounds has to be explained on the basis of a non-equivalence of the interacting protons. The usual procedure for assigning spectra is to count the number of lines and observe their relative intensity and then try to find a model consistent with both the starting material and the products which gives the correct number and intensity of lines. In the application of this procedure several difficulties arise. It is difficult in counting lines to know which of the weaker lines are (a) part of the desired isotropic spectra, (b) weak anistropic components resulting from partial alignment of the crystallites comprising the samples, which are polycrystalline powders, or (c) due to small amounts of other radicals. The intensity ratios are not easily determined. The actual absorption-intensity ratios depend only on the degeneracy of the spin states. However, the apparent line-intensity ratios depend on the line width and the degree of overlap of the spectra as well as on the actual absorption-intensity ratios. Deuteration provides a check on radical assignments made on the basis of the apparent line-intensity ratios. Deuterium has a smaller nuclear magnetic moment than hydrogen. Substituting it for a proton reduces the size of the electron-nuclear interaction so much that the hyperfine spectrum is effectively lost.

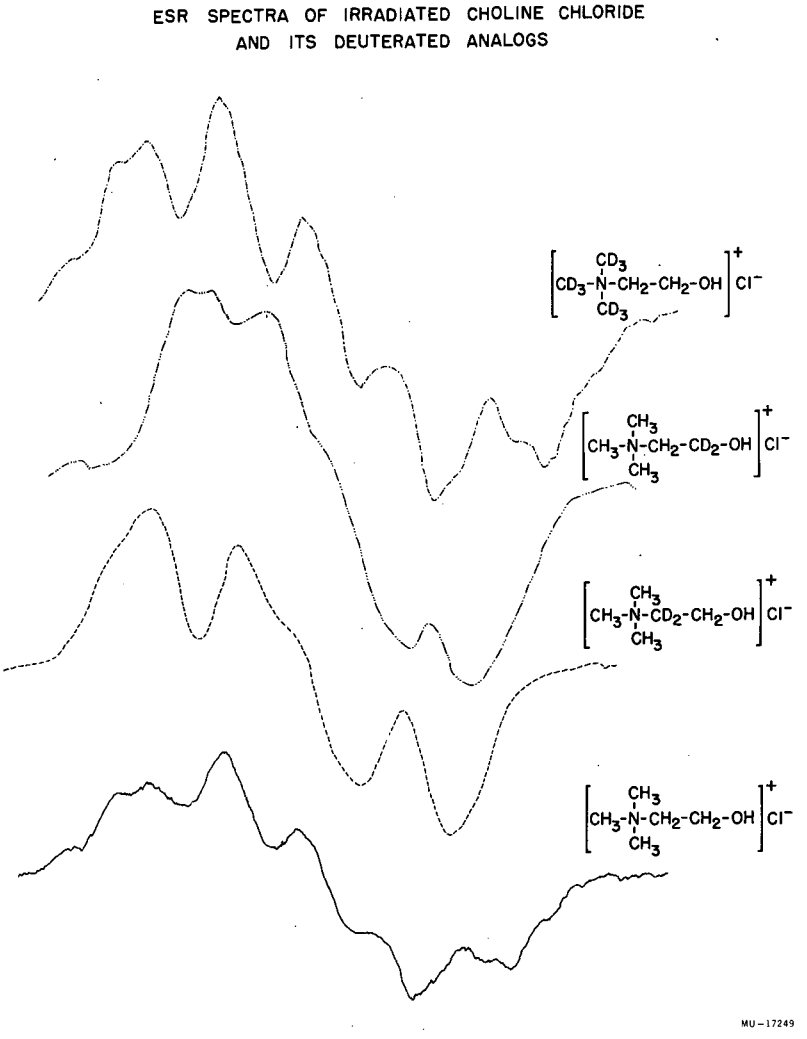

Fig. 12. ESR Spectra of irradiated choline chloride and its deuterated analogs.

This procedure also has to be considered with some reservations, as deuteration can change the reaction kinetics and equilibria considerably and either of these changes may cause a completely different radical to be observed. When a sample in which all the electrons are paired is irradiated and radicals are formed, radicals must be formed in pairs (including e^- as a radical). This does not assure that the ESR spectrum will reveal a pair of radicals. One radical may have such a broad line that it escapes detection and only the other radical is seen. Another possibility is that one radical is more mobile and hence has decayed via dimerization more rapidly than the observed radical. Low-temperature studies would allow this type of system to be studied.

One other experimental fact needs to be included before we consider applicability of the combinations of two radical spectra in Table VI. Over a wide range of radical concentrations the spectra of the decaying radicals in irradiated choline chloride stayed the same. Thus if two radicals produced the observed spectra they either (a) decayed independently at exactly the same rate, or (b) they were present initially in the same concentration and decayed by mutual annihilation. The two-radical hypothesis requires equal numbers of both radicals and thus equal areas for both spectra. Actually, the rough intensity measurements used in this discussion are the differences in maximum slopes of an absorption-type curve, and are observed as the differences between maximum and minimum amplitudes on the derivative-type spectrum. Thus, the apparent intensity ratios could vary considerably if two radicals with different line widths were involved. Within any one spectrum in Fig. 12 there is little evidence of radicals with different line widths, although the line widths and shapes indicate nonequivalent protons. In Fig. 12 it can be seen that deuteration of the 2-position changed the spectrum from a five-line to a three-line spectrum, so that only those cases in which one spectrum is a triplet are included in Table VI. Only one case of the two radicals with different g values (Table VI, Case E) was included. This can be ruled out because it would require that the deuterated (1- and 3-position) analogs give asymmetrical spectra of two peaks, one of which has a 1:2:1 hyperfine

Table VI

Combinations of overlapping spectra to produce a five-line spectral intensity distribution

	Species	Spectra
Case A	2 equivalent H^+	1 2 1
	2 non-equivalent H^+	1 1 1 1
		1 2 2 2 1
Case B	N	2 2 2
	1 H^+	3 3
		3 2 2 2 3
Case C	2 equivalent H^+	1 2 1
	1 H^+	2 2
		1 2 2 2 1
Case D	2 equivalent H^+	1 2 1
	2 equivalent H^+	1 2 1
		1 1 4 1 1
Case E	2 equivalent H^+	1 2 1
	2 equivalent H^+	1 2 1
		1 2 2 2 1

splitting and the other none. The one other case that can give a triplet for either 2- or 3-deuterated analogs (or quadruplets if the protons are not exactly equivalent) is Case D in Table VI with a 1:1:4:1:1 intensity distribution. This can be ruled out as too different from the observed spectrum. The observed intensity ratio of undeuterated choline chloride (Fig. 7) is about 1:3:3:3:1. The better resolved 1-deutero case suggests 1:2:2:2:1. Case B (Table VI) fails to fit intensity ratios for either the undeuterated or deuterated compound. Cases A and C (Table VI) are potential candidates that can fit the undeuterated case and the 2-deutero case but fail to fit the 3-deutero case. This consideration cannot completely rule out these cases, as isotope effects are always possible and may give a different radical for this case. The fact that the radiation damage of 3-deutero choline chloride is only one-half as great as the rest of the deuteroanalogs and of the normal compound itself offers some support for this argument.

The single-radical hypothesis (including the case in which two radicals exist but only one spectrum is observable) also deserves consideration. Table IV illustrates the spectra that can arise from simple combinations of hydrogen and nitrogen nuclei interacting with an unpaired electron. Cases D and H for proton interactions alone, and Cases J and L for interaction with N nuclei and protons, all give five lines. Since Cases J and L involve only a single hydrogen nucleus and a single nitrogen nucleus, they are ruled out by the absence of any nitrogen triplet splitting (1:1:1 intensity ratio) in deuterated-analog spectra. In the remaining two cases, D, with a 1:2:2:2:1 intensity ratio from three protons, comes closer to fitting the spectrum of undeuterated compound than Case H, with a 1:4:6:4:1 ratio from four equivalent protons. Either case fits the triplet spectrum of the irradiated 2-dueterated choline analog. Only Case H (Table IV) can explain the poorly resolved triplet from the 3-deutero analog. In order to use Case D it is necessary to invoke isotope effects and argue that the radical produced has a different structure when the choline analog is deuterated in the 3-positions. In light of the poor resolution, the intensity measurements are believed to be the weakest feature in this

work. It should be further pointed out that the 1:4:6:4:1 intensity ratio for the four equivalent protons (Case H) is based on the integrated absorption intensity. The four- and sixfold intensities result from four- and sixfold energy-level degeneracies. Any small difference in the size of the electron-proton interaction acts to broaden the line and reduce the difference in slopes. This has no effect on the slope of the end lines, where there is no degeneracy, and has the maximum effect on the slope of the sixfold degenerate level. This may easily cause a 1:4:6:4:1 intensity distribution to appear as a 1:2:2:2:1 maximum slope-difference ratio. In fact, the shape of the central line of the triplet of the irradiated 2-deutero analog clearly shows some nonequivalence of the protons in the 3-position. The whole spectrum nearly qualifies as a quadruplet from two nearly equivalent protons. There appears to be about a 30% difference in the hyperfine interaction of the two protons.

A Radical Model for the ESR Data

The following model is consistent with all the observed spectra when the above broadening mechanism is considered:

$$(CH_3)_3\overset{+}{N}{:}CH_2{:}CH_2OH\ \ Cl^- \rightsquigarrow (CH_3)_3\overset{+}{N}\cdot \text{ and } :CH_2\cdot\ CH_2O\text{--}H\text{--}Cl^-$$

This model assumes that the nitrogen radical is not seen either because of excessive broadening by the nine protons in the 1-position or because of coupling between the positive nitrogen and the lattice. Likewise the 4-position proton is not seen as a result of a weakening and broadening of its interaction by hydrogen bonding to the Cl^-. The hydrogen bonding or other crystal forces can provide the necessary activation energy to prevent immediate recombination of the radicals. This model is not inconsistent with the known products of irradiation, i.e., trimethylamine hydrochloride and acetaldehyde.

ELECTRON-SPIN RESONANCE STANDARDS

Spectrometer Sensitivity

The amplitude of the signal observed in electron-spin resonance (ESR) spectroscopy is dependent not only on the number of unpaired electrons in the sample but also on other factors related to the spectrometer, sample, and the sample container. The microwave dielectric losses in the sample and holder represent non-ESR absorption and frequently determine the merit factor, or Q, of the loaded microwave cavity. Aside from dielectric losses, ESR absorption is due to magnetically induced electron-spin transitions and varies as the square of the magnetic component of the microwave field (H_1). For this reason, displacement of the sample and holder from the point of maximum H_1 weakens the signal in two ways. First, since the point of maximum H_1 is the null point of the electric field, the displacement may increase the dielectric losses with the resultant lower Q. Secondly, H_1 is reduced, and this also reduces the instrument sensitivity. A simplified derivation of this situation, given in Ingram's book[52], is

$$dv = \frac{(NP)^{1/2} Q_0 x''}{V} ,$$

where

N = impedance of the wave guides feeding the cavity,

P = microwave power level propagated through the system,

Q_0 = power circulation per power dissipation per cycle in the loaded cavity,

x'' = imaginary component of the magnetic susceptibility of the sample,

V = effective volume of the cavity,

dv = the change in microwave output voltage due to x''.

Although this formula is derived for the simple transmission cavity and direct absorption-type system shown in Fig. 13, it applies equally well to the derivative system shown in Fig. 13, which is a schematic diagram of the type of equipment used in this work. The equipment using magnetic modulation and a lock-in amplifier is capable

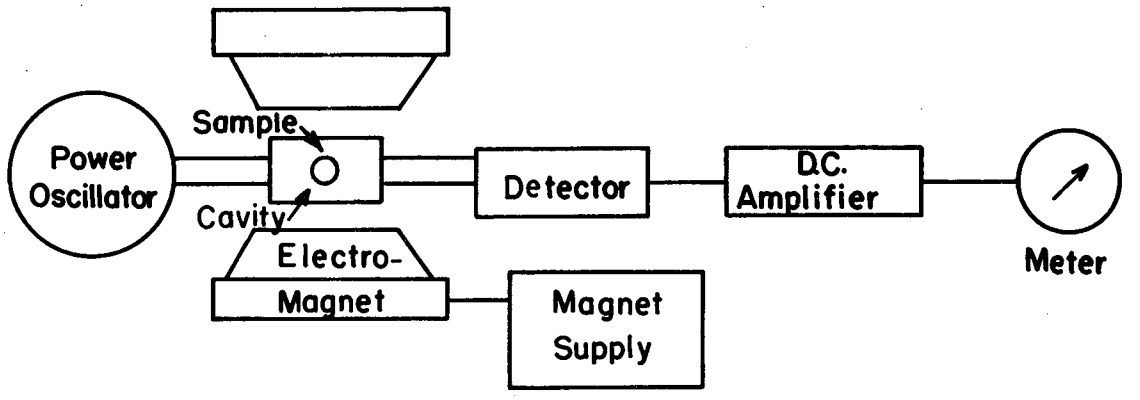

MU-12658

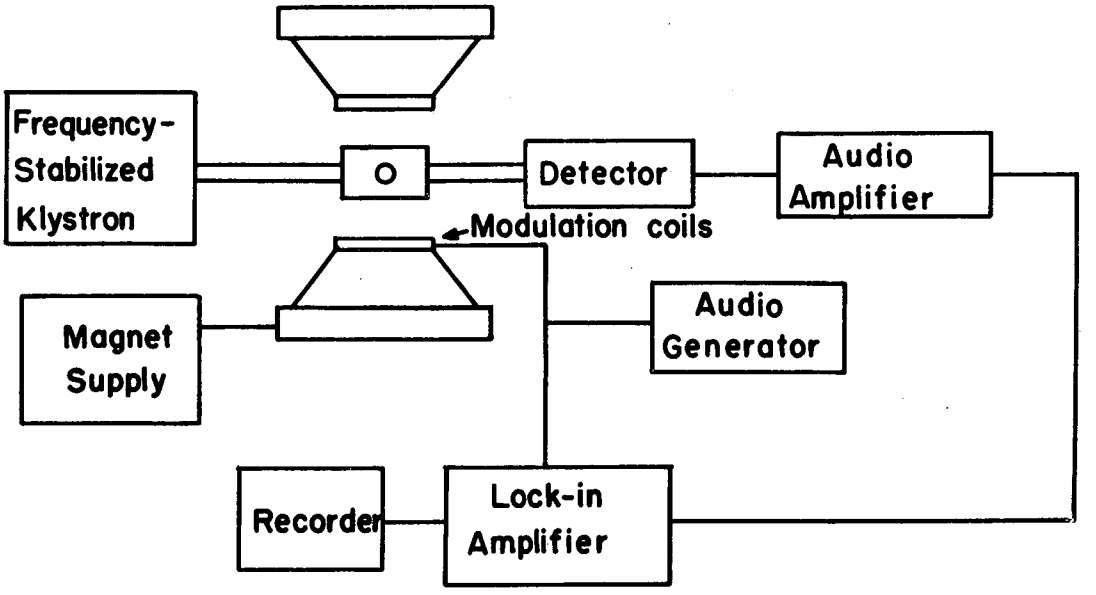

MU-12659

Fig. 13. ESR spectrometers.
Upper: An absorption type ESR spectrometer utilizing a transmission cavity.
Lower: A derivative-type ESR spectrometer utilizing a transmission cavity.

of giving the same height of signal with a H_s (i. e. magnetic modulation amplitude) of half the signal width, but is frequently used with a much smaller amplitude of magnetic modulation. With the smaller values the shape of the signal approximates a derivative curve of the absorption, as shown in Fig. 14. The advantage of this system is that the lock-in amplifier rejects practically all the noise components not of the modulation frequency. In this way, the signal-to-noise ratio of the system can be improved by a factor of ten or more over measuring the microwave absorption directly. It is clear from the large number of parameters discussed in the foregoing paragraphs that the simplest and most accurate way to make quantitative ESR measurements is to compare the signal from a sample with that from an internal standard (i. e. a standard dispersed in the sample) containing a known number of unpaired electrons.

There is yet another reason for searching for a convenient standardization system. The lack of a universally accepted standards system hampers the comparison of results in different laboratories. Although no single standard can ever be ideal for all types of ESR measurements, a very convenient system might still find general acceptance and thus alleviate this problem.

Internal Standards

Now that the reasons for an internal standard have been pointed out, it is valuable to consider what physical and chemical properties are desirable in an internal standard. Since such a standard is one that is mixed with the sample, the resulting spectrum is a superposition of the individual spectra. For this procedure to be most useful, it is necessary that the standard's spectrum be easily distinguished from that of the sample. In the ideal arrangement, the spectral peaks are separate and distinct and do not overlap each other. The center of an ESR spectrum is designated by a g value, defined as

$$g = \frac{h\nu}{\mu H} \quad ,$$

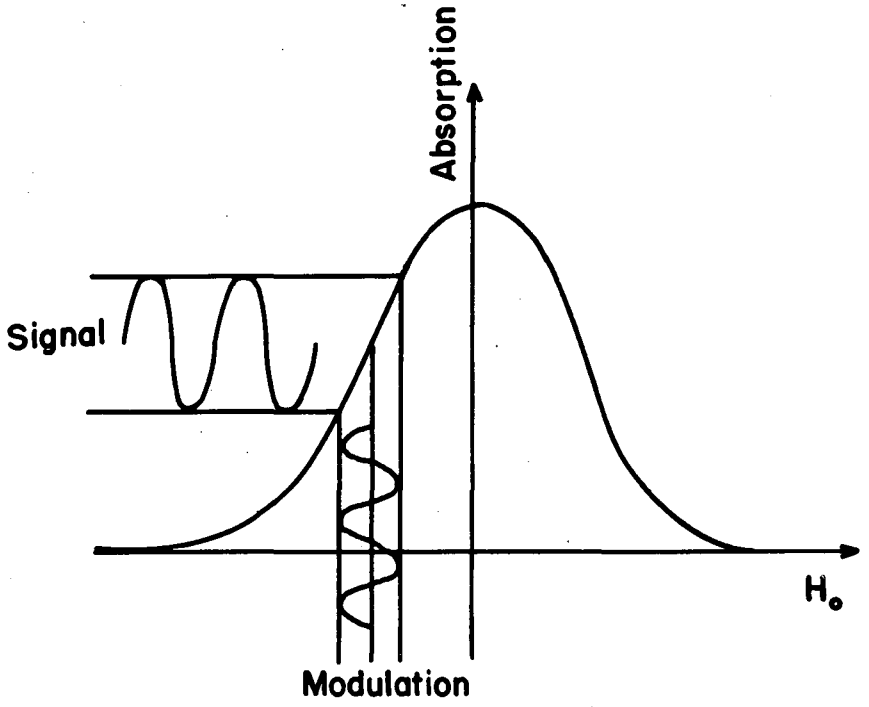

Fig. 14. Relationship of signal to modulation in a magnetic modulation-Type ESR system.

where h = Planck's constant,

ν = the microwave frequency,

μ = magnetic moment of a Bohr magneton,

H = magnetic field for the center of the spectrum.

Unfortunately, all the organic free radicals that have been observed have nearly identical g values. They vary over a range of only 0.1% about a mean value of 2.0023.[53]

In order to avoid overlapping of spectral peaks of the standard and sample it is necessary either to use a standard with a g value somewhat above or below this range, or to use a standard whose spectrum is split by hyperfine structure so that a large area of the spectrum around g = 2.00 is nonabsorbing. Another important requirement is that the standard be stable and not undergo, during handling, any change (e.g., crystal form or oxidation state) that would affect its spectrum. Further, a standard should be in a convenient physical form; a standard that requires sealing in glass, or other special handling, loses much of its usefulness.

The above considerations apply mainly to a secondary standard. The important considerations for a primary standard are different. Here, the absolute accuracy with which the chemical composition can be determined and the extent of the theoretical understanding of the spectrum are of the greatest importance. The shape of the spectrum is relatively unimportant. It should not be too broad, and should be easily distinguished from the secondary standard.

Previous ESR Standards

It is instructive to consider a few materials used as ESR standards in the current literature as background for the present standards work. The only organic free radical that has found any great use as an ESR standard is diphenylpicrylhydrazyl, usually designated as DPPH.[54] DPPH does not have an ideal spectrum for a secondary standard. The solid has a line width of 3 gauss, and is centered at g = 2.0037. In dilute solution the spectrum widens out to a width of about 50 gauss and shows a nearly resolved five-line hyperfine structure. Although DPPH is reasonably stable and can be handled in the open, in

10^{-4} M solutions it reacts appreciably with impurities in the common solvents, and in normal handling it decomposes at the rate of several percent a day. In bright light the DPPH is completely decomposed in a few hours. Because of its chemical reactivity it is difficult to obtain in pure form, and optical extinction coefficients for DPPH can be found in the literature ranging from 6500 to 14,500.[55, 56] The worst drawback to the use of DPPH as a primary standard is our inability to determine its chemical purity and hence to know how many free radicals, or unpaired electrons, we have in a sample. Its reactivity, and lack of an ideal spectral pattern, weigh against its use as a secondary standard. The chief asset of the DPPH is its availability. It is easily made from commercially available diphenylpicrylhydrazine,[57] or the radical itself may be purchased.[58]

In the transition groups of the periodic table are a large number of elements that form chemically stable compounds while retaining an incomplete inner shell containing unpaired electrons. These compounds show ESR absorption and can be used as standards. They differ from organic radicals in several ways: first, in chemical stability and, second, in that their g values are generally anisotropic and have a wide range of values.

Single crystals of $CuCsSO_4 \cdot H_2O$ have been used as an ESR standard.[59] Since the g values show a 15% anisotropy, one is restricted to the use of single crystals to keep a reasonable line width, but the anisotropy permits one to shift the absorption peak away from that of the sample by oriented the single crystals in the field. The need to implant orineted single crystals of standard in the sample is the only objectionable feature to the use of this standard. However, this particular requirement greatly restricts its use. This method can be easily applied only to large, stable samples.

Development of a Secondary ESR Standard

Since our kinetic studies of the radiation-induced radicals in choline chloride had to be done on small samples of 5 to 10 mg in sealed 3-mm tubes, the use of single crystals for standards was not practical. Also the mixing of the samples and any standard was not a good procedure, since this would superimpose the spectrum of the radiation damage in the standard on the desired spectra of the sample and standard. Next to mixing of the sample and standard the best geometry is obtained by jacketing the sample with a thin sleeve of the standard. Organic radicals like DPPH were considered for this purpose since they can be dissolved in plastics or paraffin and fabricated into the desired cylindrical shape, but their lack of chemical stability and their nonideal spectra more than outweighed their advantages and, consequently, they were not used as standards. There are two transition elements with a stable half-filled 3d shell; these are Mn^{+2} and Fe^{+3}. These constitute a special case since a half-filled 3d shell has no orbital angular momentum. Thus, long spin-lattice relaxation times, with correspondingly narrow lines, are expected for dilute solutions; also isotropic g values are expected since there are no orbital moments to couple with the spin moment. Although both Mn^{+2} and Fe^{+3} have been extensively investigated, only Mn^{+2} gives a useful hyperfine structure of six lines. This hyperfine structure results from the nuclear spin of 5/2 for the Mn^{55} nucleus.[60] No nuclear hyperfine splitting has been observed for iron compounds.[52]

Mn^{+2} as an ESR Standard

A system that has an isotropic g value is capable of giving narrow lines in polycrystalline form. If such a system can be found with a hyperfine splitting that gives a spectrum with no peaks at g = 2.0023, one has a very convenient system for a secondary standard which avoids the use of oriented single crystals and may be dispersed in a plastic medium of a convenient shape. Mn^{+2} has good chemical stability and meets these requirements when sufficiently dilute in a cubic lattice. Lattices of lower symmetry than cubic show crystal field splitting, and lose their desirable spectral features.[61]

A molar dilution of somewhat more than 1 atom of Mn^{+2} to 1000 of diluent is necessary to avoid dipole-dipole broadening of the lines. For this reason, the majority of my efforts were devoted to finding a suitable cubic lattice in which to dilute Mn^{+2}. In order to have the spectra of other paramagnetic impurities low compared with the Mn^{+2}, they must be present in less than 1 part per million (mole ratio) in the cubic lattice used as a diluent for the Mn^{+2}.

Natural MgO (periclase) has been used as a secondary standard and can be obtained from mineral suppliers.[62] Finding a natural ore with a suitable concentration of Mn^{+2} and sufficiently low concentrations of all the other paramagnetic impurities is difficult and does not produce a standard of general availability. Because of the importance of achieving widespread acceptance of a single standard, a search was undertaken to find a source of pure MgO or a method of purification of the commercially available Mg compounds, and a suitable procedure to fabricate it into the cubic MgO after a small amount of Mn^{+2} was added.

Figure 15 shows the spectrum of Mn^{+2} in MgO made from Baker & Adamson reagent-grade $MgCl_2 \cdot 6H_2O$. Although this was the purest commercial source of a Mg salt found, it had about 25 ppm of Mn^{+2} and 1000 ppm of other paramagnetic impurities; their presence is shown by the structural features indicated by the arrows. In Fig. 16 is shown the spectrum of the same material containing 125 ppm of Mn^{+2}; that is, to the 25-ppm material was added 100 ppm (mole basis) of Mn^{+2}. The level of impurities is still objectionable, therefore a purification with metallic Mg was used to remove the paramagnetic impurities below the levels that are observable with our spectrometer. The spectrum of the standard material finally used is shown in Fig. 17. This standard consisted of 2 mg of Mn^{+2}-treated MgO dispersed in 10 mg of polyethylene and fabricated into a small cylinder 3 mm in diameter. The Mn^{+2} was at a molar dilution of 1 to 5000 in the MgO, and the MgO was made from a solution of Baker & Adamson $MgCl_2 \cdot 6H_2O$ which had been purified with Mg metal. After addition of the $MnCl_2$ it was precipitated with ammonia, and heat-treated as described in the experimental section.

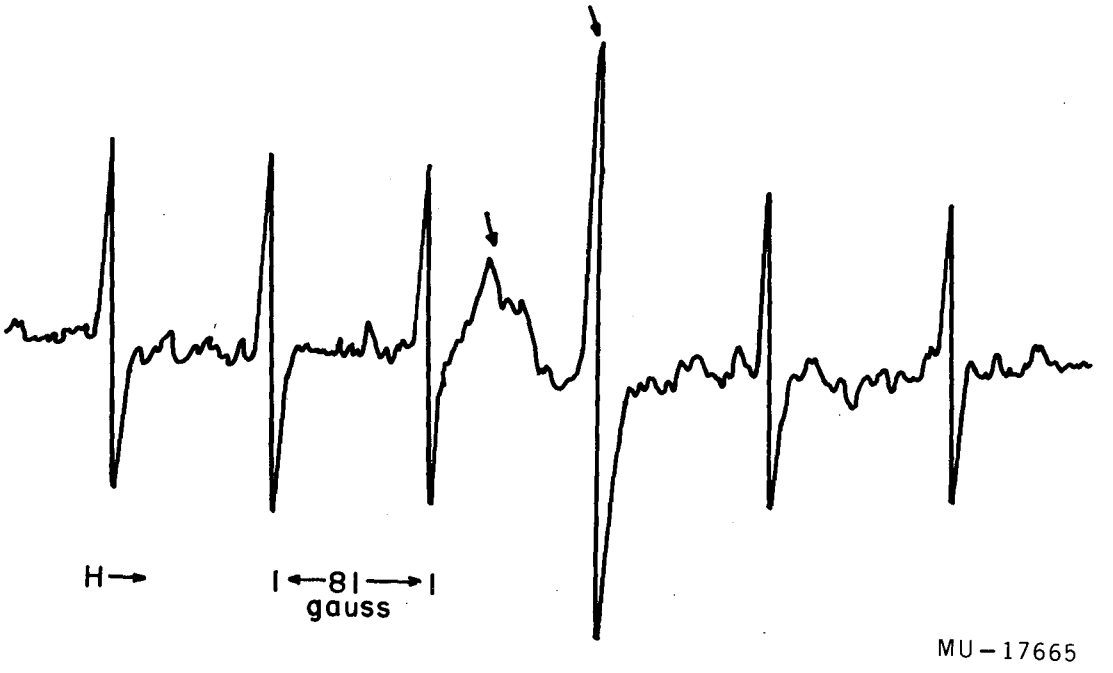

Fig. 15. ESR spectrum of MgO made from Baker & Adamson reagent-grade $MgCl_2 \cdot 6H_2O$.

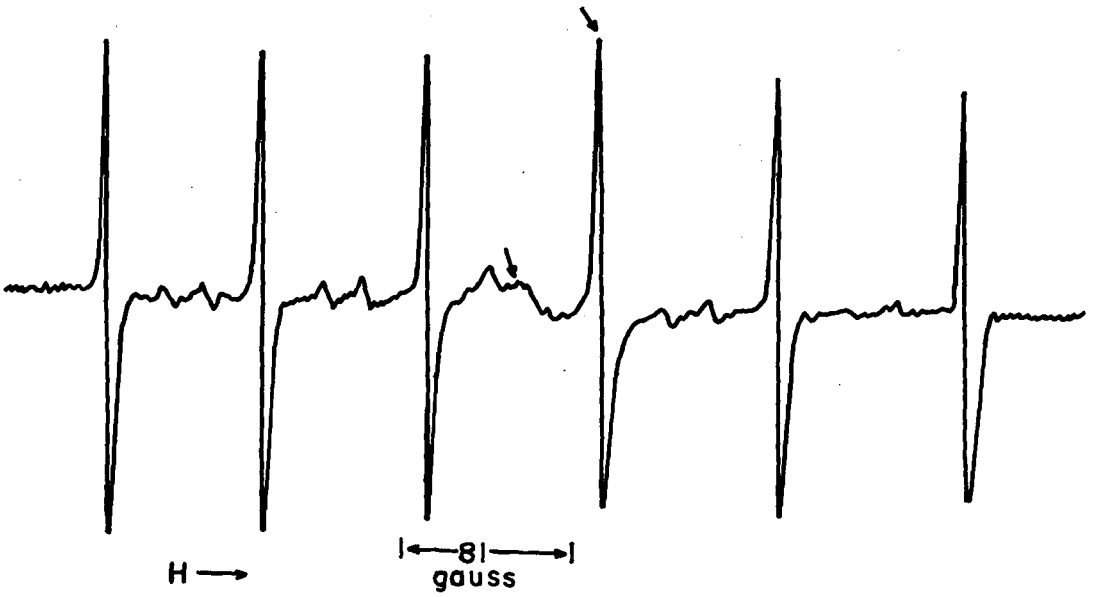

Fig. 16. ESR spectrum of a solid solution containing 120 molar ppm of Mn^{+2} in MgO made from Baker & Adamson reagent-grade $MgCl_2 \cdot 6H_2O$.

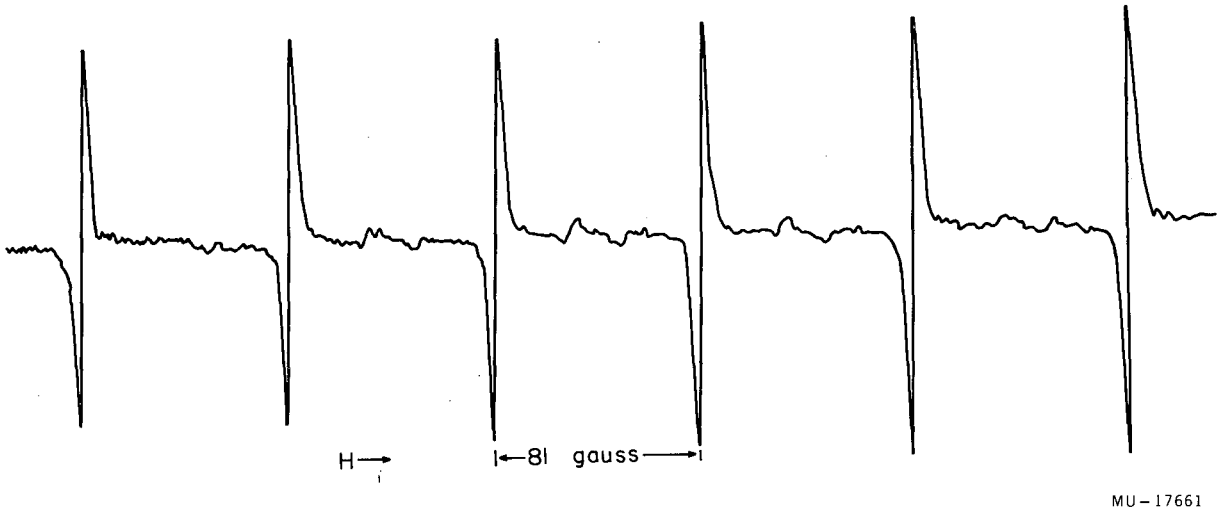

Fig. 17. ESR spectrum of a solid solution containing 200 molar ppm of Mn^{+2} in MgO made from purified $MgCl_2$ solution.

The concentration of one part in 5000 was a compromise between resolution and an effort to reduce to a minimum the material put in the cavity. The small satellite peaks visible between the major peaks are not understood, but their uniform spacing relative to the Mn^{+2} spectrum and their correspondence in intensity with the Mn^{+2} concentration, indicate they are a part of the Mn^{+2} spectrum. The dilute solid solution of Mn^{+2} in MgO has been used only as a secondary standard and has been calibrated with aqueous solutions of manganous chloride, assuming the aqueous Mn^{+2} exists in the $^6S_{5/2}$ state.[63] This procedure makes unimportant any variability in the coprecipitation or reduction steps.

Although the cubic MgO appears quite stable to hydration to $Mg(OH)_2$ at the usual laboratory temperatures and humidities, the conditions required for this transition have been clarified by three experiments. First, when Mg metal was dissolved in 4 M $MgCl_2$ solution at 25°, a granular precipitate formed which gave an ESR signal for the Mn^{+2} and the other impurities exactly like the dehydrated cubic standard. Secondly, gelatinous freshly precipitated $Mg(OH)_2$ from a Mn^{+2}-treated $MgCl_2$ solution fails to give a Mn^{+2} spectrum after drying at 120°, and requires high-temperature dehydration and reduction with H_2 or CH_4 (to prevent the oxidation of the Mn^{+2}) to yield the Mn^{+2} spectrum. Thirdly, the treated MgO lost its Mn^{+2} spectrum after a week under water at 40°. These three observations indicate the transition $MgO + H_2O \longrightarrow Mg(OH)_2$ takes place between 25° and 40°. Thermodynamic calculations of this transition are not definitive as they indicate a 40° transition temperature if the product is the amorphous $Mg(OH)_2$, but if the trigonal form "brucite" is considered the product, the calculated transition temperature is 20°. The experimental evidence indicates 40° as the correct transition temperature. When the standards are dispersed in polyethylene film, they should be protected by the polyethylene from hydration even in the event of exposure to 100% humidity at 40°.

The various attempts to obtain MgO with a very low level of paramagnetic impurities are summarized in Table VII.

Table VII

Paramagnetic impurity levels in MgO from various sources

Source of Mg	Reaction to make MgO	Estimated impurity level (Molar ppm)
Mallinckrodt analytical-grade metal	Burned in air	1000
C-reduced and distilled metal from Dr. Kelly, U. S. B. M.	Burned in air	20
Merck MgO, U. S. P. grade	Used as is	20
(CH_3MgI)	Hydrolyzed with H_2O	30
Mg from methoxide	Used as is	15
Brucite	Dehydrated	1000
Dense hard burnt MgO (from $Mg(NO_3)_2$)	Used as is	20
Baker $MgCl_2 \cdot 6H_2O$	Precipitated with KOH (analytical grade)	Broad line 10,000 Narrow line 20
Baker $MgCl_2 \cdot 6H_2O$	Precipitated with NH_4OH	0.5
Baker $MgCl_2 \cdot 6H_2O$	Scavenged with Mg metal before precipitation with NH_4OH	Below detection, i. e., < 0.05

Other Standards Systems

The systems that were tried other than Mn^{+2} in MgO are summarized in Table VIII. Of the systems listed, two deserve further comment. First, the Mn^{+2} in oven-dried $SrCl_2$ gives the attractive spectrum in Fig. 18 and is exceedingly easy to prepare. Exposure to atmospheric humidities causes a transition from the cubic $SrCl_2$ to the rhombic $SrCl_2 \cdot 6H_2O$ with the complete loss of the Mn^{+2} spectrum. Even trace amounts of water change the shape of the spectrum and give rise to a broad underlying signal as shown in Fig. 19. This material might have some application for short-term use as a calibrated secondary standard, but its instability argues against its general acceptance as a standard. Secondly, the DPPH would be a useful primary standard if an unambiguous optical-extinction coefficient could be established. Although its ESR spectrum is not convenient for a secondary standard and would badly overlap the spectra of most organic radicals, it would be convenient to calibrate Mn^{+2}-treated MgO standards.

Table VIII

Systems unsuitable for use as ESR standards

Sources of Unpaired Electrons	Diluent	Spectrum	Disadvantages
Nitrosyldisulfonate	water	3 lines each 2 gauss wide & 13 gauss apart	Poor chemical stability
Diphenylpicrylhydrazyl (DPPH)	benzene	5 lines nearly resolved over 50 gauss	Inability to get an exact assay, only moderate chemical stability, and a nonideal spectrum
Manganous salts of:			
phthalic acid	dioxane		No spectrum found
benzoic acid	dioxane		
palmitic acid	dioxane		
$MnCl_2$	ppt from H_2O in $PbNO_3$	6 lines each 24 gauss wide	Poorly resolved spectrum
$MnCl_2$	ppt from H_2O in PbF_2	6 lines each 36 gauss wide	Poorly resolved spectrum
$MnCl_2$	fused in $SrCl_2$	6 narrow lines over one broad line	Unsatisfactory spectrum
$MnCl_2$	fused in $BaCl_2$	single 245-gauss line	Unsatisfactory spectrum
$MnCl_2$	ppt from H_2O in CaF_2	weak broad line	Unsatisfactory spectrum
$MnCl_2$	fused in NaCl	weak 6 lines	Inferior to Mn^{++} in MgO system and metastable
$MnCl_2$	oven dried $SrCl_2$	6 lines each 9 gauss wide over 89-gauss interval	Deliquescent and metastable

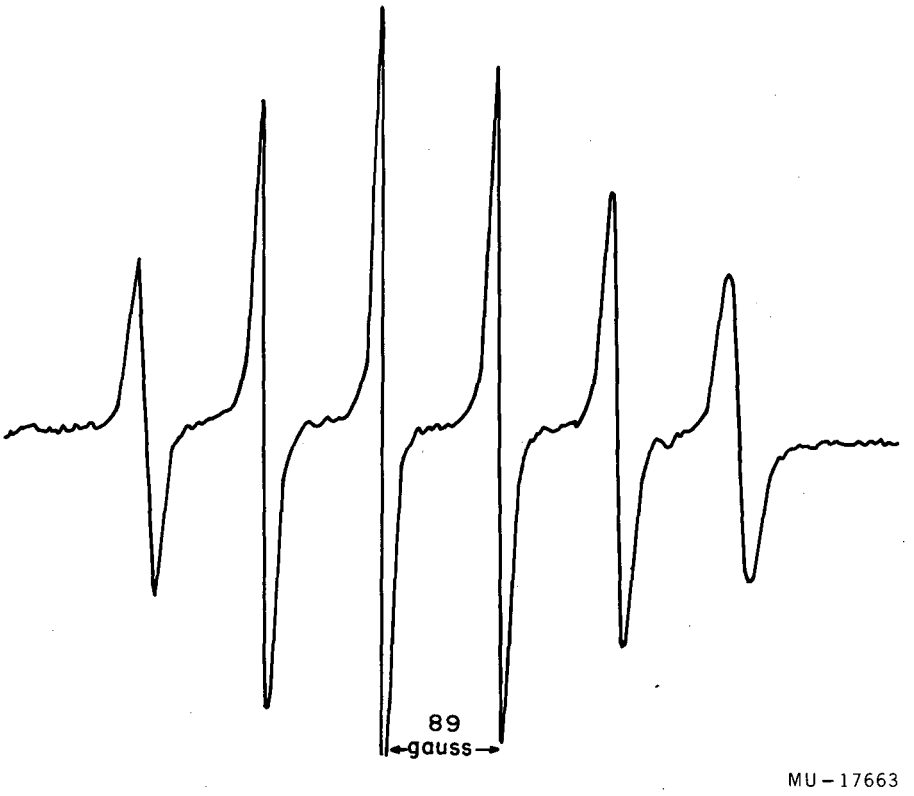

Fig. 18. ESR spectrum of a solid solution of 200 molar ppm of Mn^{+2} in $SrCl_2$.

MU-17662

Fig. 19. ESR spectrum showing the start of the effect of traces of water on a solid solution of 200 molar ppm of Mn^{+2} in $SrCl_2$.

Comparison of Standard and Sample

The need for a suitable internal-standard system has been discussed in the first section and the development in the second section. It remains now to discuss the theory and mathematical tools need to compare the number of spins in the sample and standard through their spectra. If an ESR spectrometer system such as that in Fig. 13 were used with a bolometer detector, a spectrum of the power absorbed versus H_0 could be obtained. The relationship for a simple absorption system of this type is given by Silsbee[59] as

$$\int_0^\infty x''_{H_0}\, dH_0 = N \frac{g_1^2}{g_0} \left[\frac{\pi h \nu \beta S(S+1)}{6 k T}\right] = \int_0^\infty \frac{\text{Power absorbed} \cdot dH_0}{H_1^2 \nu \pi}$$

where power absorbed $= x''_{H_0} H_1^2 \nu \pi$,

x'' = the imaginary component of the susceptibility,

H_1 = the magnetic component of the microwave field at the sample,

ν = the frequency of the microwave field,

H_0 = the static magnetic field at the sample,

N = the number of paramagnetic ions,

g_1 and g_0 = the diagonal elements of the g tensor in the directions of H_1 and H_0, respectively

h = the Planck constant,

k = the Boltzmann constant,

T = the absolute temperature,

β = the Bohr magneton,

S = the total spin-quantum number (i.e., n/2 for n electrons).

Practically the same relationship is derived in greater detail by Ingram.[62]

The above expression may be simplified to the following, since we are interested only in relating standards and samples both of which have isotropic g values exceedingly close to 2.0023:

$$\frac{N_r}{N_A} = \frac{(S_A)(S_A + 1)\int_0^\infty x''_A \, dH}{(S_r)(S_r + 1)\int_0^\infty x''_r \, dH},$$

where the subscripts r and A stand for the unknown radicals and standard materials. S_A for a dilute aqueous solution of manganous salts has been well established as 5/2 by Gouy balance measurements.[63] Hence, when manganese solutions are used to calibrate organic radicals with one unpaired electron the relationship becomes

$$N_r = N_A \frac{.35\int_0^\infty x''_A \, dH}{3\int_0^\infty x''_A \, dH}.$$

When a derivative spectrometer of the type shown in Fig. 13 is used, the $\int_0^\infty x'' \, dH$ is not directly available from the spectrum, but may be calculated. When the spectrometer is operated with a small value of H_S relative to the spectral features of interest, a good derivative of x'' (i.e., $\frac{dx''}{dH_0}$) is rendered. It is obvious that a double integral will give the values needed for the calculation (i.e. $\int_0^\infty \int_0^\infty \frac{dx''}{dH} dH^2 = \int_0^\infty x'' dH$). An entirely equivalent operation is the calculation of the first moment of the derivative curve, which is illustrated in Appendix 3. It is not so apparent that these calculations are valid with values of H_S so large that the spectrum is no longer a derivative of x''. That this is the case is illustrated in Appendix 4 by applying Andrew's calculation[64] to a first-moment or double-integral calculation of the spectrum from a derivative-type ESR machine. In Appendix 5 the limitations of a fast approximate method are shown. If the maximum slope is multiplied by the square of the distance between the points of maximum slope, a value is obtained that is a good approximation to the area of a Gaussian curve and is dimensionally correct. Let this quantity be called the approximate area of the integral curve and designated as AAI. Although this quantity is very easily calculated

from the derivative spectrum, its accuracy is very dependent on the curve shape. Most of the ESR spectra have shape functions that lie somewhere between a Lorentzian and a Gaussian shape. It has been shown that the Lorentzian shape may arise from broadening due to interaction of the of the unpaired electrons with precessing local dipoles and the Gaussian shape may arise from interaction with static local fields.[66] In Appendix 5 the AAI method has been applied to these shape functions. The sizable correction indicated for the Lorentzian-shape curve indicates the limitations in its use. This method is useful only if one knows that the same shape function describes all the spectra being compared or knows the necessary corrections. If the shape function is not known, a first-moment or double-integral calculation is necessary, and this can then be related to the AAI or more simply to the peak height. As long as the shape function is unchanged the number of radicals can be related simply through the peak height after the initial calibration. Although the shape function of the spectrum is independent of H_S when the line width is much larger than H_S, the shape function becomes very sensitive to H_S when the line width is comparable to or smaller than H_S.

Experimental Procedure

Baker & Adamson reagent-grade magnesium chloride was made up as a 4 M solution with distilled water. Two hundred and fifty ml of this solution was reacted with 12 grams of Mallinckrodt analytical-reagent-grade magnesium metal turnings in a stirred beaker at 25°. The magnesium dissolved, and granular magnesium oxide precipitated from the solution. When the magnesium was about half dissolved, the purified magnesium chloride solution was separated from the MgO precipitate by filtration. The purified magnesium chloride solution was then treated with some 0.1 M solution of Mallinckrodt analytical-reagent-grade manganese chloride to give a mole ratio of 1 part to 5000 of Mn^{+2} to Mg^{+2}. The treated solution was then precipitated with large excess of B. & A. reagent-grade ammonium hydroxide. The precipitated $Mg(OH)_2$ was centrifuged at 3000 g, then reslurried and washed with water in the amount of nine times the volume of the

compacted solids. This procedure was repeated three times. The washed $Mg(OH)_2$ was dried in an oven at 120° and then ground into a fine powder. This powder was heated for 2 minutes to 1000° in a Meker burner, and then allowed to cool under hydrogen or natural gas. The solid was used where a standard in powder form was desirable. It was fabricated in a film by dispersing it in powdered polyethylene and rolling it flat between sheets of Teflon film on a hot plate at 200°. The sheet was cut into strips of suitable length and these were likewise welded into small cylinders by pressing against the heated Teflon on the hot plate.

If only a qualitative standard is needed, or if the standard is going to be calibrated against some other primary standard such as DPPH or an aqueous solution of Mn^{+2} or $CrCl_3$, then a very simple method is available for preparing the Mn^{+2} in MgO standards. The purified 4 M $MgCl_2$ solution is treated with $MnCl_2$ to give approximately a 2×10^{-4} M concentration of Mn^{+2}. This solution is then precipitated by treatment with Mg metal. A granular precipitate of MgO containing the Mn^{+2} as a dilute solid solution forms and is evolved. Because of the granular cubic form of the precipitate, and the reduction conditions used, there is no need for centrifugation and for the subsequent heat treatment and reduction.

The solid solution of Mn^{+2} in $SrCl_2$ was very simply made. Twenty microliters of 0.1 M $MnCl_2$ solution was mixed with 10 ml of 2 M $SrCl_2$ solution and then evaporated to dryness in an oven at 120°.

DISCUSSION AND INTERPRETATION OF CHEMICAL AND ESR MEASUREMENTS ON IRRADIATED CHOLINE CHLORIDE

Radicals

Ever since the original observation that radicals accompanied radiation damage in irradiated choline chloride[6] it had been assumed that the radicals were the agent responsible for the propagation of the chain decomposition. After the ESR hyperfine-structure work was completed two programs were set up to test this assumption. The first program was to study the effects of radiation dose and chain-propagation time on the chain decomposition of irradiated choline chloride. The second program was to study the radical-production efficiency (G_r) of different radiation doses and also the radical-decay rates as a function of dose and decay time. It was hoped that, with these two pieces of data, either a relationship could be established between the radical concentration and the chemical damage rate, or they could be shown to be unrelated. It should be emphasized that only the lack of relationship between radicals and damage could be conclusive. Even if a relationship could be established it would remain a difficult problem to prove that the radicals were the chain-propagating species rather than a side product of an ionic chain-reaction sequence.

Since it had been previously established that the chain-propagation reaction and radicals were stable for extended periods of time at -196° the samples were irradiated and stored at this temperature unitl convenient times to start the ESR and chemical-damage studies. Because the chemical analyses destroyed the samples the ESR radical data were taken on the 300-hour samples only. It became apparent only after most of the data were taken that some crystal changes were occurring at higher radiation-damage levels, and these changes obscured the original research objective, which was the comparison of radical concentrations and the chemical damage rates.

Chemical Data

Figures 20 and 21 and Table IX contain data from three different experiments. The irradiations were all done with 4.0- to 4.5-Mev electrons and the chemical analyses were all done by the volatile-amine method. The samples were irradiated near, and stored at, -196° to

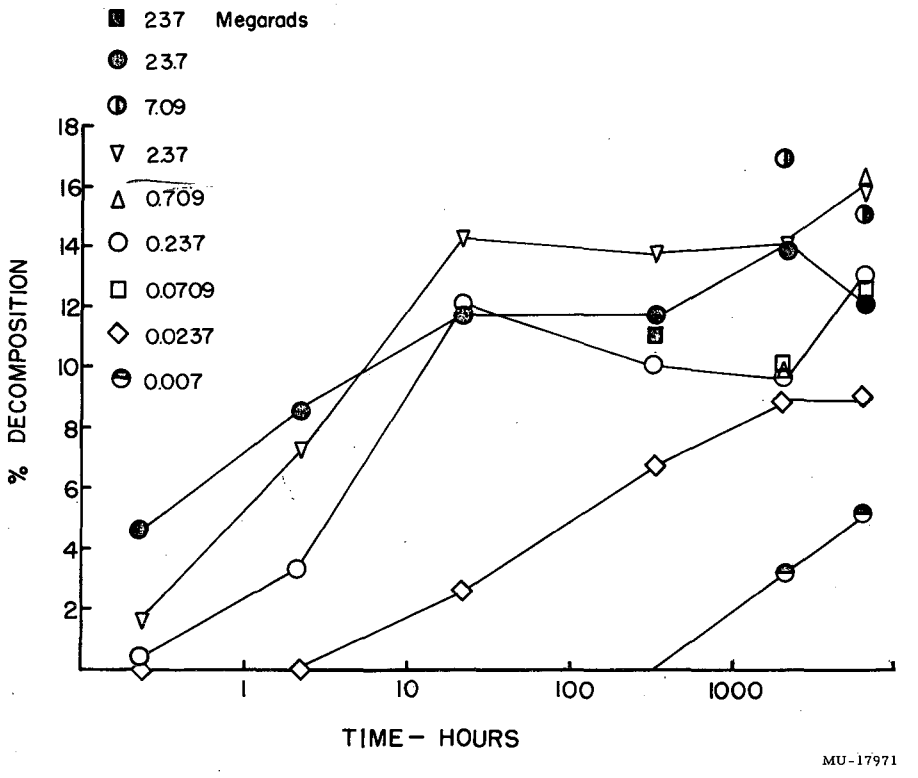

Fig. 20. Decomposition (%) of irradiated choline chloride as a function of chain-propagation time and radiation dose.

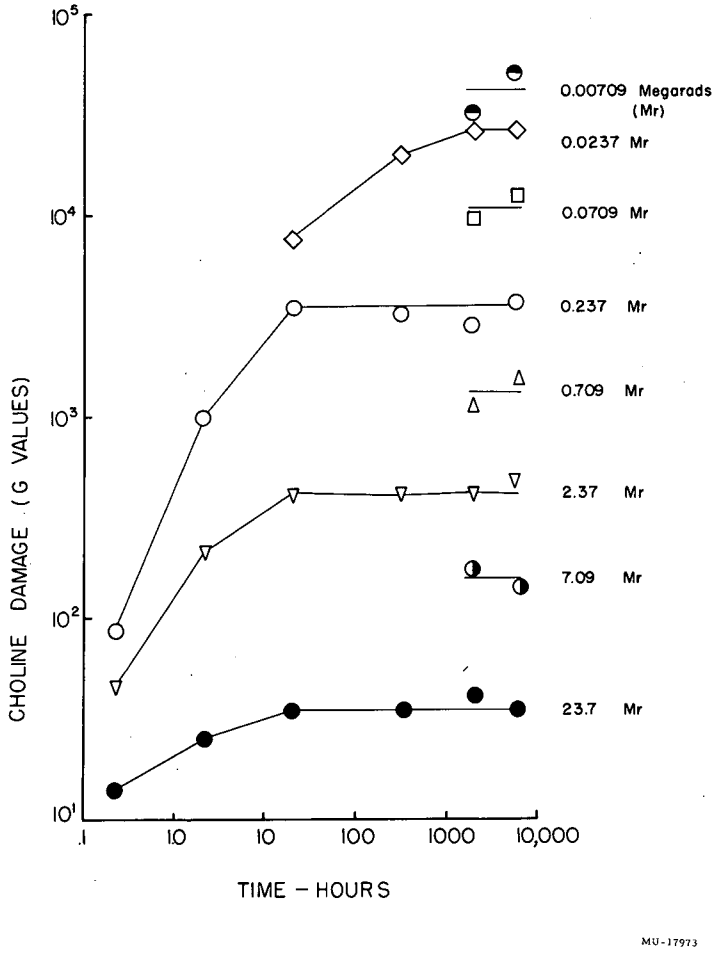

Fig. 21. G values of irradiated choline chloride as a function of chain-propagation time and radiation dose.

Table IX

Percent decomposition and G values of irradiated choline chloride as a function of dose and radical-propagation time

Dose	Time (hr) for chain propagation											
	0.235		2.16		20.9		33.6		2110		6320	
(megarads)	%	G	%	G	%	G	%	G	%	G	%	G
2.37×10^{2}							11.2	3.3				
2.37×10^{1}	4.6	13.4	8.6	25.0	11.9	34.7	11.9	34.7	14.1	41.2	12.2	35.5
7.09×10^{0}									17.0	165	15.1	147
2.37×10^{0}	1.6	46.5	7.4	215	14.3	416	13.8	402	14.2	413	16.1	469
7.09×10^{-1}									10.6	1130	16.5	1600
2.37×10^{-1}	0.3	87	3.4	990	12.1	3520'	10.2	3260	9.7	2820	13.1	3790
7.09×10^{-2}									9.9	9600	12.7	12,300
2.37×10^{-2}	0.0	--	0.0	--	2.7	7850	6.9	20,000	9.0	26,200	9.1	26,500
7.09×10^{-3}									3.3	32,100	5.3	51,500
2.37×10^{-3}	0.0	--	0.0	--	0.4	--	0.4			--		--

prevent chain decomposition during irradiation and storage. All the chain-propagation reactions occurred at room temperature.

The first irradiation provided the data for chain-propagation times of 6000 and 2000 hours. The results were somewhat surprising. Although the radiation doses ranged from 23.7 to 0.00709 megarads (Mr), all the samples receiving more than 0.00709 Mr had nearly the same decomposition, that is, between 9% and 17%. Lemmon[67] and later Serlin[7] and other workers had observed radiation-damage levels of 50% and more when their samples were continuously irradiated (beta and gamma irradiation had both been used) at room temperature. This led to a hypothesis that the chain-propagating species was formed in very high yield and saturated at low doses. Under this hypothesis the damage was about the same because the initial concentration of the chain-propagating species was the same. Since the radical G value was known to be constant (i. e., the concentration proportional to the dose) over a large part of this dose range, these initial data seemed to indicate that the radicals were not involved in the radiation-induced damage.

When the second irradiation was done the samples were first used to get the ESR data in Figs. 22, 23 and 24, then they were analyzed to get the 300-hour results in radiation-damage data. The saturation hypothesis was badly weakened by the declining values observed on the 0.0237-Mr curve. In the third irradiation the data for 20, 2, and 0.2 hr was obtained. It was now apparent that the saturation effect was time-dependent, and the saturation hypothesis became completely untenable. It became necessary to reconsider an earlier idea. The alternative to saturating the level of the propagating species is an accumulative mechanism such as a progressive build-up of stress in the crystal with increasing damage until at about 8% damage a change in crystal structure begins and the new changed geometry inhibits chain propagation, thus preventing further crystal damage. Any explanation of the saturation effect observed with low-temperature irradiations must also be consistent with the higher radiation-damage levels (i. e., up to 60%) that Lemmon[67] and other workers have observed when choline chloride was continuously irradiated for relatively long times at room temperature.

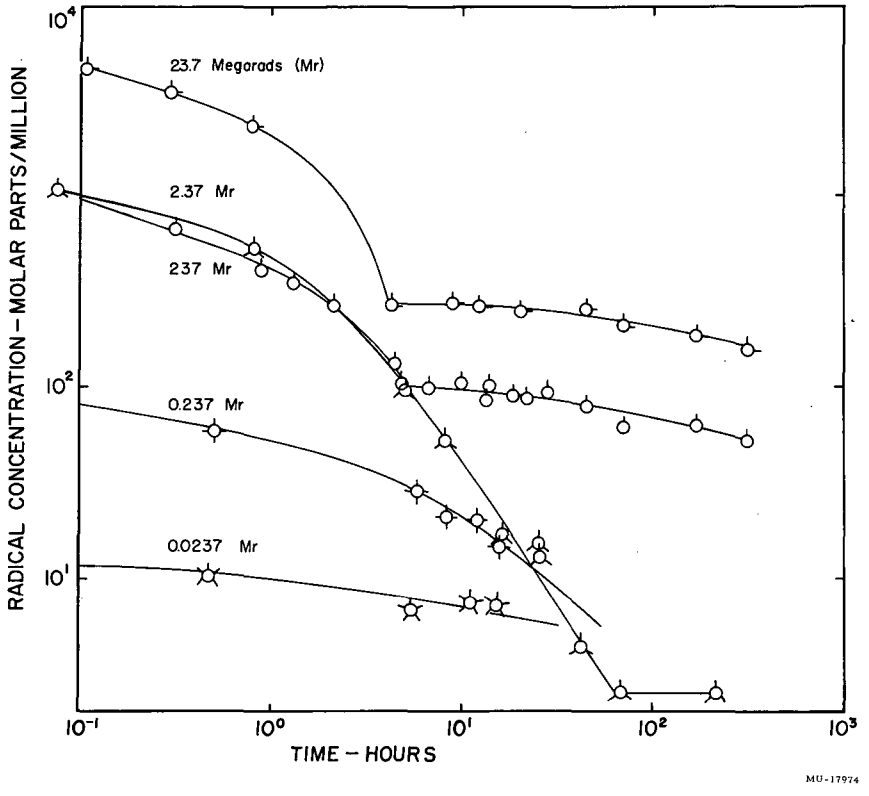

Fig. 22. Radical concentrations in irradiated choline chloride as a function of radiation dose and chain-propagation time.

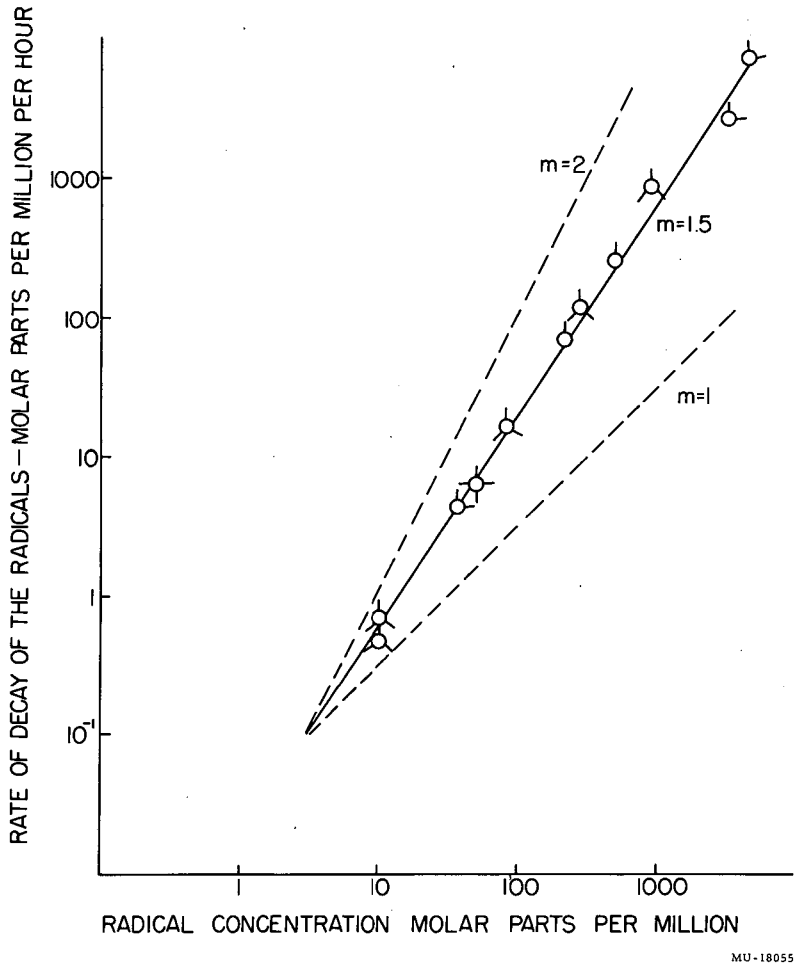

Fig. 23. Radical decay rate as a function of radical concentration in irradiated choline chloride.

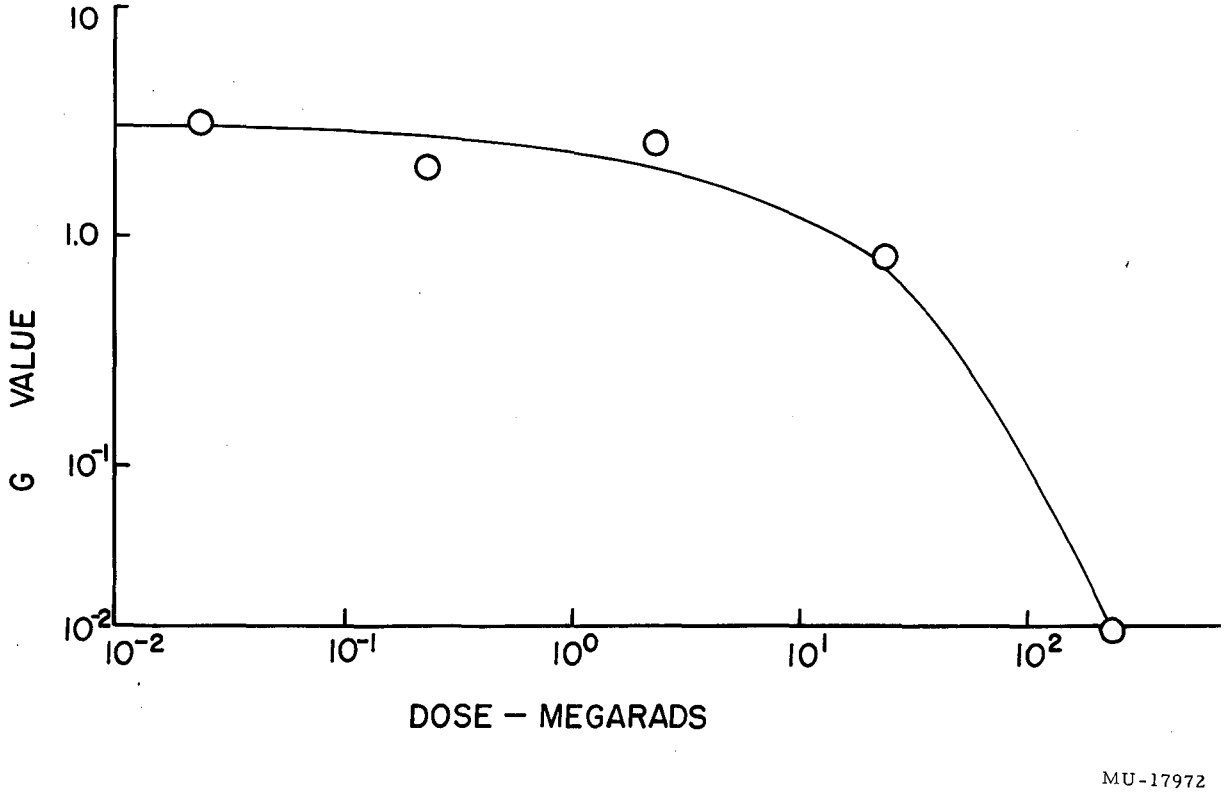

Fig. 24. Radical G values as a function of dose.

Two obvious alternatives present themselves. First, the saturation effect may be due to a phase change in the crystal. A phase change in choline chloride from orthorhombic to cubic at 73° to 78° has been reported by Collin.[8] He suggested this as an explanation for the unexpected radiation stability of choline chloride at 150° reported by Serlin.[7] To make this phase hypothesis consistent with the observations for continuous room-temperature irradiations, it is necessary to assume that further irradiation not only generates radicals but also anneals or catalyzes the annealing of the crystal, and thus relieves the stress and strain caused by the crystal damage. Seitz's "hot spot" theory[68] suggests this type of radiation annealing. This annealing promotes a phase change back to the orthorhombic structure in which the radicals can propagate. The second alternative is to assume that the change in crystal structure that is responsible for the saturation effect is the formation and splitting away of a second phase comprised of the damaged crystal structure. This hypothesis assumes the radicals are isolated either in the body of the second phase or at the interface and thus are no longer able to propagate and cause further damage. Since the damaged areas are almost certainly adjoining in the crystal, it would be more surprising if they did not split away from the body of the crystal. The physical appearance of irradiated choline chloride crystals changes as radiation damage develops. The choline chloride gradually changes from a transparent to a translucent material. This can be consistent with either of the above mechanisms but does not particularly favor either.

In retrospect, the data upon which Figs. 20 and 21 are based is not ideal for testing a kinetic law. In order to cover as wide a range of variables as possible, both the radical concentrations and chain-propagation times were changed in stages by factors of 10. This has resulted in data in which only one or two points out of each set lie in the 1% to 5% damage range where the data are well above analytical error and below the postulated crystal-damage effect. Consequently, there is a very inadequate amount of data to test the kinetic model developed in the next section on ESR measurements.

ESR Data

The data in Fig. 22 were obtained by ESR measurements on irradiated choline chloride samples. The techniques used are completely described in the section on Quantitative ESR Standards and Measurements. Since the data in Fig. 22 came from the samples used for the 300-hour points in Fig. 21 only radiation damage from this set of points can be accurately compared with the ESR data. The other points allow only an approximate comparison, owing to variations in individual treatment and handling; however, the same general patterns should hold. The three samples given the largest doses, 237, 23.7, and 2.37 Mr, all show sharp breaks in their rates of radical decay that roughly correspond to the flattening of the G-value curves in Fig. 21.

The appearance of lower radical concentrations in the sample given 237 Mr than that given 2.37 Mr deserves some additional comment. Immediately following irradiation this sample developed a different appearance from any of the other samples. The larger crystals were already translucent and the sample appeared to have an increased distribution of very finely divided sample. A radical G_r value of 3.5 (from the low dose range of Fig. 22) is a reasonable index of the efficiency of initial radiation damage (i. e., non-chain-produced) in choline chloride. A calculation of total initial radiation damage expected with 237 Mr dose leads to about 11% initial decomposition. Since this damage level is well into the range where the anomalous saturation effects have been observed with the chain damage process, it is not surprising to find a discontinuity in the relationship between radical concentration and radiation dose at this dose level, even without the chain-damage mechanism.

The highest concentration of radicals observed was about 0.6%. Since 237 Mr gave a lower radical concentration, a maximum exists somewhere between the doses of 23.7 and 237 Mr. The ability of the crystal structure to tolerate 0.6% radicals is in itself informative about the origin of the radicals. It is difficult to conceive of toleration of this high a radical concentration in any other way than as stabilized radical pairs. This leads to the schematic picture in Mechanism 1A for the initial radiation-damage act. Radiation produces an

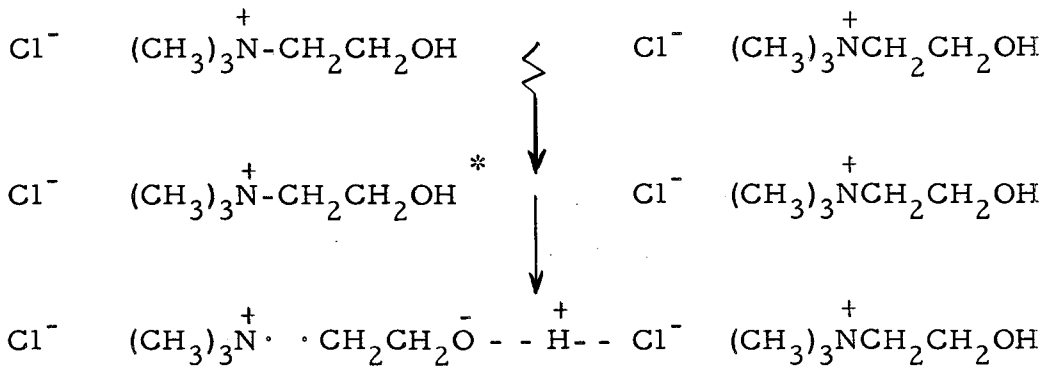

Mechanism 1-A: a model for the formation of stabilized radicals in irradiated choline chloride.

Where

choline chloride = Cho,

$(CH_3)_3\overset{+}{N}\cdot\cdot CH_2CH_2O\text{--}H\text{----}Cl^-$ = $\dot{Cho}\cdot$,

$CH_3\dot{C}HOH$ = $\dot{A}cH_2$,

CH_3CH_2OH = EtOH,

CH_3CHO = AcH,

G_c = $\frac{\text{molecules choline destroyed}}{\text{100 ev ionizing radiation absorbed}}$,

G_r = $\frac{\text{radicals produced}}{\text{100 ev ionizing radiation absorbed}}$,

one can write

$$Cho \rightsquigarrow Cho^* \xrightarrow{\text{fast}} \dot{Cho}\cdot, \tag{0}$$

$$\dot{Cho}\cdot \xrightarrow{k_1} (CH_3)_3\overset{+}{N} + \dot{A}cH_2, \tag{1}$$

$$\dot{A}cH_2 + Cho \xrightarrow{k_2} (CH_3)_3\overset{+}{N}H + AcH + \dot{A}cH_2, \tag{2}$$

$$\dot{A}cH_2 + \dot{Cho}\cdot \xrightarrow{k_3} (CH_3)_3\overset{+}{N}H + AcH + \dot{A}cH_2, \tag{3}$$

$$\dot{A}cH_2 + \dot{A}cH_2 \xrightarrow{k_4} EtOH + AcH; \tag{4}$$

assuming steady-state conditions, we have

$$\frac{d\dot{A}cH_2}{dt} = 0 = k_1\,\dot{Cho}\cdot - k_4(\dot{A}cH_2)^2 \tag{5}$$

or

$$\dot{A}cH_2 = \left(\dot{Cho}\cdot\ \frac{k_1}{k_4}\cdot\right)^{\frac{1}{2}}, \tag{6}$$

which leads to

$$\frac{d\dot{Cho}\cdot}{dt} = -k_1(\dot{Cho}\cdot) - k_3(\dot{Cho}\cdot)(\dot{A}cH_2) = -k_1(\dot{Cho}\cdot) - k_3\left(\frac{k_1}{k_4}\right)^{\frac{1}{2}}\left(\dot{Cho}\cdot\right)^{\frac{3}{2}}. \tag{7}$$

The observed 3/2 order requires

$$\left(\dot{Cho}\cdot\right)^{\frac{1}{2}}\ \frac{k_3}{(k_4)^{\frac{1}{2}}} \geq (k_1)^{\frac{1}{2}} \tag{8}$$

or

$$\left(\dot{Cho}\cdot\right)^{\frac{1}{2}} \geq \frac{(k_1 k_4)^{\frac{1}{2}}}{k_3},$$

$$-\frac{dCho}{dt} \approx \frac{dAcH}{dt} = k_2(\dot{A}cH_2)(Cho) + k_3(\dot{A}cH_2)(\dot{Cho}\cdot) + k_4(\dot{A}cH_2)^2$$

$$= k_2\left(\frac{k_1}{k_4}\right)^{\frac{1}{2}}\left(\dot{Cho}\cdot\right)^{\frac{1}{2}}(Cho) + k_3\left(\frac{k_1}{k_4}\right)^{\frac{1}{2}}\left(\dot{Cho}\cdot\right)^{\frac{3}{2}} + k_1(\dot{Cho}\cdot). \tag{9}$$

Since the dose is given by $D_{mr} = \dot{Cho}\cdot\ \frac{69}{G_r}$ and $-\frac{dG_c}{dt} = \frac{dCho}{dt}\ \frac{69}{D_{mr}}$

$$-\frac{dG_c}{dt} = k_2\left(\frac{k_1}{k_4}\right)^{\frac{1}{2}}\left(\dot{Cho}\cdot\right)^{-\frac{1}{2}}(G_r). \tag{10}$$

Mechanism 1-B: a kinetic model for choline chloride radiation decomposition.

In view of the good fit to the 3/2 law for the radicals and the large G value of choline damage, simplify Eqs. (7) and (9) to the following (11) and (12). In the following equations take: $\dot{Cho}_o$ as the initial concentration of $\dot{Cho}\cdot$ and Cho_o as the initial concentration of choline

$$\frac{d\dot{Cho}\cdot}{dt} = -k_3\left(\frac{k_1}{k_4}\right)^{\frac{1}{2}} \left(\dot{Cho}\cdot\right)^{\frac{3}{2}} \tag{11}$$

$$\frac{-dCho}{dt} \cong \frac{dAcH}{dt} \cong \frac{d(CH_3)_3\overset{+}{N}H}{dt} = k_2\left(\frac{k_1}{k_4}\right)^{\frac{1}{2}} \left(\dot{Cho}\cdot\right)^{\frac{1}{2}} \tag{12}$$

First integrate 1 to get a value to put in 2.

$$\int_0^t \left(\dot{Cho}\cdot\right)^{-\frac{3}{2}} d\dot{Cho}\cdot = -k_3\left(\frac{k_1}{k_4}\right)^{\frac{1}{2}} \int_0^t dt$$

$$+2\left[\left(\dot{Cho}\cdot\right)^{-\frac{1}{2}} - \left(\dot{Cho}_o\cdot\right)^{-\frac{1}{2}}\right] = +k_3\left(\frac{k_1}{k_4}\right)^{\frac{1}{2}} t$$

$$\left(\dot{Cho}\cdot\right)^{-\frac{1}{2}} = +\frac{k_3}{2}\left(\frac{k_1}{k_4}\right)^{\frac{1}{2}} t + \left(\dot{Cho}_o\cdot\right)^{-\frac{1}{2}} \tag{13}$$

$$\left(\dot{Cho}\cdot\right)^{\frac{1}{2}} = \frac{1}{+\frac{k_3}{2}\left(\frac{k_1}{k_4}\right)^{\frac{1}{2}} t + \left(\dot{Cho}_o\cdot\right)^{-\frac{1}{2}}} \tag{14}$$

Substituting (14) in (12) gives

$$-\int_0^t dCho = k_2\left(\frac{k_1}{k_4}\right)^{\frac{1}{2}} \frac{dt}{+\frac{k_3}{2}\left(\frac{k_1}{k_4}\right)^{\frac{1}{2}} t + \left(\dot{Cho}_o\cdot\right)^{-\frac{1}{2}}}$$

$$(Cho_o - Cho) = +k_2\left(\frac{k_1}{k_4}\right)^{\frac{1}{2}} \frac{1}{\frac{k_3}{2}\left(\frac{k_1}{k_4}\right)^{\frac{1}{2}}} \log\left\{\frac{\frac{k_3}{2}\left(\frac{k_1}{k_4}\right)^{\frac{1}{2}} t + \left(\dot{Cho}_o\cdot\right)^{-\frac{1}{2}}}{\left(\dot{Cho}_o\cdot\right)^{-\frac{1}{2}}}\right\} \tag{15}$$

$$(Cho_o - Cho) = 2\frac{k_2}{k_3} \log\left[1 + \frac{k_3}{2}\left(\frac{k_1}{k_4}\right)^{\frac{1}{2}} (t)\left(\dot{Cho}_o\cdot\right)^{\frac{1}{2}}\right] \tag{6} \tag{15}$$

Mechanism 1-C: approximate integration of the kinetic model.

excited lattice which leads to an excited molecule. The excited molecule has antibonding orbitals in the N-C bond and the choline disproportionates to a pair of radicals. Hydrogen bonding to the adjacent Cl^- provides a potential barrier to prevent the radical-radical recombination. The important idea of $-O--\overset{+}{H}--Cl^-$ bond in choline chloride has already been used by Senko[69] in discussing its crystal structure.

Radical-Decay Reaction Order

The order of the radical-decay reaction was investigated by measuring decay rates on the curves in Fig. 22 (prior to the curve discontinuities), and plotting the decay rate as a function of the concentration on log-log paper. Figure 23 shows these data. The points fall in a reasonably tight group about a line with a slope of 1.5 ± 0.1 and a decay rate

$$k_r = \frac{-2\ 10^{-2}}{(\text{molar ppm})^{1/2}}\ \text{hr}^{-1}.$$

Since the data are taken over a 500-fold range of radical concentration, the 3/2-order decay reaction seems well established. Furthermore, the data were taken under conditions that give rise to up to only 4% decomposition, so that the proposed mechanism also appears to be nearly independent of the damage in the crystal as long as the damage is below the saturation level.

The Role of the Radicals

At the time when the radical characterization work was in progress the role of the radicals in the radiation-initiated chain decomposition of choline chloride was not clearly understood. Since there always seemed to be radicals present when the decomposition was in progress, it was believed by the early researchers that the observed radicals must be either the chain-propagating species or a side reaction product. However, when the kinetic studies of the radical decay were completed and a kinetic model was constructed, the model that evolved had the observed radicals in the role of starting material for the chain-decomposition process rather than an intermediate in the process.

Several aspects of the data were in conflict with the old hypothesis that the observed radicals were the chain-propagating species. The

radical G values were nearly constant up to a dose of 2.37 Mr (Fig. 24), but the initial chemical G values (Fig. 21) are not only significantly different (even when normalized with the radical concentrations in Fig. 22), but they also diverge even more when the points at 2 hrs are considered. A second argument revolved around the 3/2-order decay observed with the radicals. If the observed radicals were the chain-propagating species, the chain-termination processes would determine the shape of the radical decay function. If the termination reaction was a first- or second-order process a corresponding radical-decay order would have been observed. However, a mixture of first- and second-order termination processes could have given the appearance of a 3/2-order process over a narrow concentration range. The data in Fig. 23 appear to rule out all these possibilities, since a good fit to a slope of 3/2 was obtained over a several hundredfold concentration range. Similarly, if a diffusion rate controlled the termination process then an exponential curve would have been observed. A convenient solution to this problem can be found in the classic method of Rice and Herzfeld.[70] A model based on this method was adopted, and is shown in Mechanism 1-B. This mechanism predicts a square-root dependence of the rate of decomposition on the radical concentration, and an inverse-square-root dependence of the rate of increase of the G value at low dose levels where the radical G value is constant. Thus a change of 10 in the initial radical concentration should give rise to a change in the rate of radiation damage by a factor of 3.16. A rough fit to this can be seen for the top three points of the 0.25-hr set in Fig. 20. The data in Fig. 20 also suggest that there is a linear relationship between radiation damage and the log of the chain-propagation time. Three out of four of the dose levels below 23.7 Mr show this linear relationship quite well. In Mechanism 1-C the kinetic expressions are integrated after certain simplifying assumptions have been made. The end result (i.e., Eq. (6), Mechanism 1-C) fits the observed linear relationship between damage and the log of the chain-propagation time. It is also apparent that although this expression gives the correct damage relationship for dose at short times and for time at constant dose, it

fails to fit the dose-time relationships at large time values. The equation does not fit the data in the damage-saturation areas. The failure of the integrated rate law to completely fit the data at long chain-propagation times and low doses is probably the consequence of dropping the lower-order terms to simplify the integrations in Mechanism 1-C .

EFFECTS OF ISOTOPIC SUBSTITUTION ON THE G VALUES OF IRRADIATED CHOLINE CHLORIDE

Isotopically substituted compounds have found considerable use in recent years by kineticists[71] as a means of exploring the transition state of chemical reactions. The kinetic effects of D substitution result from a reduction of the frequency of the H-molecule vibrational modes and hence a reduction of the zero-point energy levels. The rate-determining step observed here is believed to be

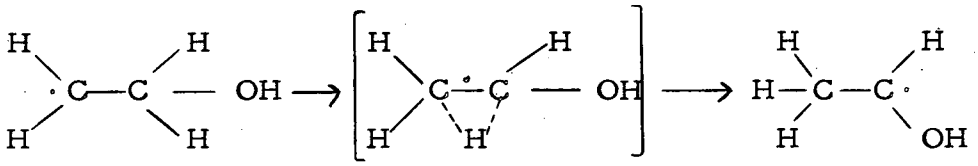

The major effect in forming the activated complex is that a bending mode of C-H (normally about 1450 cm^{-1}) goes to the zero-frequency reaction coordinate to produce a difference in zero-point energy of 610 calories between H and D. Furthermore the mass in the reaction coordinate gives a factor $\sqrt{2}$ for k_H/k_D. The net effect of this very rough evaluation is that k_H/k_D should be about 4.0 at 20°.

Experimental Details

The selectively deuterated sample material consisted of small remanent amounts of the material used in the radical-characterization work; the synthesis and characterization of these compounds has been previously described. Four to 7 mg quantities of the deuterated choline chlorides were placed in 3-mm o. d. Pyrex tubes. After the tubes were evacuated to 100 microns or less and baked out at 90° for 1 hour the tubes were sealed. The smaples were placed along the periphery of a rotating sample holder in a Co^{60} source. All the samples were exposed at room temperature to a dose rate of $9.07 \cdot 10^6$ rep/hr ($7.4\ 10^6$ rad/hr) for 13 minutes. The samples were left for 4 days at room temperature, and then analyzed by the reineckate analysis method. The results are shown in Table X.

Table X

G values of irradiated deuterium-substituted choline chlorides

Compound	% Decomposition	G Value
$(CH_3)_3\overset{+}{N}CH_2CH_2OH\ Cl^-$	17.6	746
$(CH_3)_3\overset{+}{N}CH_2CD_2OH\ Cl^-$	7.2	302
$(CH_3)_3\overset{+}{N}CD_2CH_2OH\ Cl^-$	16.0	670
$(CD_3)_3\overset{+}{N}CH_2CH_2OH\ Cl^-$	20.0	798

Discussion

This experiment preceded the studies of decomposition and radical concentration as a function of dose and chain-propagation time. The data in Table X seemed to indicate the involvement of an O-methylene proton in the rate-limiting step of the reaction.

The subsequently observed dose-saturation effect makes this hypothesis much more tentative. The decompositions (%) of the Co^{60} γ-irradiated samples are in the same range where the damage saturation effect has been observed. If this saturation occurs in the same way for Co^{60}-irradiated samples as it did with 4.5-Mev e^--irradiated samples, then these decompositions are being limited not by the kinetics but by the crystal's damage tolerance. On the other hand, it is reasonable to assume that the well collimated electrons from the linear accelerator and the random excitation of a uniform γ flux from the Co^{60} source produce different radical distributions in the irradiated samples. The damage-saturation effect may be quite sensitive to the distribution of the damage in the crystal. With these considerations in mind it is apparent that extrapolation of 4.5-Mev e^--irradiation effects to Co^{60} irradiations may not be justified, and damage saturation may occur at a higher level or not at all. In this case the involvement of the O-methylene proton in the rate-limiting step of the chain decomposition, as previously discussed, is indicated.

FUTURE INVESTIGATIONS

Although a number of unusual and interesting aspects of the radiation damage process in choline chloride have been revealed in this investigation, there remain many facets of this process that are worth exploring. The following is a brief list of experiments that will either fill in gaps in our present knowledge of radiation damage in choline chloride, or provide a more complete test for the model that has been proposed.

1. It is desirable to get more kinetic data in that range of damage in which the crystal is less than 2% damaged. This is well below any damage-saturation effect and should be useful to test the proposed model.

2. An extension of Experiment 1 to selectively deuterated compounds will allow an unambiguous probing of the activated state.

3. The proposed chain termination via disproportionation of two radicals is pure speculation. The disproportionation was preferred to a dimerization, which would produce vicinal glycol, because it requires only a H^+ and e^- exchange. The vicinal glycol formation requires the close approach of two properly oriented radicals. Both types of products have been observed in alcohol-irradiation experiments by McDonnell and Newton.[47] Because the disproportionation reaction involves the movement of much more mobile species it was preferred for this solid-state reaction. Actual experiment is the only way to determine the chain-termination reaction. A C^{14}-labeled tracer study using carrier techniques to isolate the termination products seems the most reasonable approach to this problem.

4. Another area that justifies additional investigation is the proton rearrangements that occur in the radiation-induced decomposition of choline. This is best investigated by deuterium or tritium tracer work with selectively substituted compounds.

5. The dose-independent damage-saturation phenomenon should be further investigated. It would be very interesting to see what effect previous radiation damage has on subsequent radiation-induced radical formation and chain decomposition. The effects of different ion track

densities from different types of ionizing radiation, and the relative effectiveness of surface damage (i. e., from soft x-rays) versus damage throughout the choline chloride still need investigation.

6. It is not known whether the chain decomposition occurs in one, two or three dimensions. It is similarly not known whether the original damage sites are randomly located or have a more specific distribution in or on the crystal. The high concentrations of radical pairs would seem to indicate the random case. Some of these questions might be best approached by low temperature (-196^{o}) x-ray diffraction studies. The low temperature provide a way to block further chain decomposition damage during the x-ray diffraction study. Since the damaged choline chloride gradually becomes translucent during the chain decomposition, light scattering experiments should provide considerable information on the shape and distribution of the damaged areas in irradiated choline chloride.

ACKNOWLEDGMENTS

I would like to express my deepest appreciation for the inspiration and assistance given to me by Professor Melvin Calvin, Dr. Richard M. Lemmon, and their colleagues of the Bio-Organic Group.

Many others contributed to the completion of this program. The advice and constructive criticisms of a large number of the faculty members of the chemistry department were especially helpful. The expert assistance of Dr. Ruddy Johnston and Bill Evert with their linear accelerator greatly advanced the sample irradiations. Lastly the Lawrence Radiation Laboratory as a whole deserves credit for its role in providing both the facilities and financial assistance that made this work possible.

This work was done under the auspices of the U. S. Atomic Energy Commission.

APPENDIX 1

Electron Linear Accelerator Dose Calculations

From Feather's Rule,[72] $R = 0.543E - 0.160$, the energy lost by an electron in traversing a thin section of target is

$$\Delta E = \frac{\Delta R}{0.543},$$

or the total energy lost by a number of electrons $\Delta E_t = \frac{PXQ_sA}{0.543}$.

Since radiation dose is defined as energy absorbed per unit mass of material, the dose is

$$D = \frac{\Delta E_t}{PXA} = \frac{Q_s}{0.543}.$$

For Q_s in microcoulombs/cm^2 this becomes (since 1 microcoulomb = 0.625×10^{13} electrons)

$$D = Q_{sc} \frac{0.625 \times 10^{13}}{0.543} = 1.15 \times 10^{13} Q_{sc},$$

and for D_{mr} in megarads it is (since 1 Mev/g = 1.6×10^{-14} megarad)

$$D_{mr} = Q_{sc}(1.15 \times 10^{13})(1.6 \times 10^{-14} \text{ megarad}) = 0.185\, Q_{sc},$$

R = the range, in the target, in g/cm^2, of an electron with energy E,

ΔR = the range, in g/cm^2, corresponding to a loss of energy ΔE by an electron

E = energy of an electron, in Mev,

ΔE = energy loss, in Mev, by an electron in traveling a range ΔR g/cm^2,

E_t = energy lost (Mev) by Q_sA electrons in traversing a thin section of X cm and density P,

Q_s = total number of electrons put through the target, in units of electrons/cm^2,

Q_{sc} = number of electrons put through the sample, in units of microcoulombs/cm^2,

A = target area, in cm^2,

X = thickness of a thin target, in cm,

P = the density of the target material, in g/cm^3,

D = radiation dose, in Mev/g,

D_{mr} = radiation dose, in megarads.

APPENDIX 2

G Values for Electron Bombardment with Linear Accelerator

G is defined by $G = \frac{\text{molecules decomposed}}{\text{100 electron volts absorbed}}$, according to dose relationship derived in Appendix I.

$$G = \frac{\frac{PS}{100 \text{ mol wt}} \; 6.02\times10^{23}}{1.15\times10^{13}\times Q_{sc}\times10^{4}\, S}$$

$$G = \frac{P\times5.2\times10^{4}}{Q_{sc}\times\text{mol wt}} = \frac{P\;\; 9.63\times10^{3}}{D_{mr}\times\text{mol wt}}$$

and

$$G_{\text{choline}} = \frac{P\times69.0}{D_{mr}} \;,$$

where

P = % decomposition of the sample,

S = sample weight, in grams,

mol wt = molecular weight of the sample,

Q_{sc} = surface charge through sample, in microcoulombs/cm^2,

D_{mr} = dose, in megarads.

APPENDIX 3

First Moments of Derivative Functions

The first moment of $g'(H)$ is defined by

$$ {}_1S' = \int_{-\infty}^{+\infty} H\, g'(H)\, d\, H = \int_{-\infty}^{+\infty} H\, d\, g(H) $$

where $g(H)$ is a shape function of a curve, and $g'(H)$ is its derivative. Integrating by parts gives

$$ \int_{-\infty}^{+\infty} H\, d\, g(H) = H\, g(H) \Big|_{-\infty}^{+\infty} - \int_{-\infty}^{+\infty} g(H)\, d\, H. $$

If $g(H)$ converges at least as rapidly as H^{-} as for example, if $g^{-1}(H)$ can be represented by a nonalternating series containing terms of the first or higher powers -then

$$ H\, g(H) \Big|_{-\infty}^{+\infty} \equiv 0, $$

$$ {}_1S' = \int_{-\infty}^{+\infty} H\, g'(H)\, d\, H = \int_{-\infty}^{+\infty} H\, d\, g(H) = - \int_{-\infty}^{+\infty} g(H)\, d\, H - \int_{-\infty}^{+\infty} \int_{-\infty}^{+\infty} g'(H)\, d\, H^2. $$

APPENDIX 4

Use of Double-Integral or First-Moment Calculations on the Output of a Derivative ESR Spectrometer

Define an output voltage $v = g(H)$ where $g(H)$ is the shape function of the absorbing system and H is the magnetic field. When H is modulated, giving $H = H_0 + H_m \sin W_{mt}$, we have

$$v_0 = g(H_0) + \sum_{P=1}^{\infty} \frac{H_m \sin^P W_{mt}}{p!} \left(\frac{d^P g(H)}{d H^P} \right)_{H_0} ,$$

by a Taylor expansion. This output may be represented as a sum of a series of sinusoidal waves which are harmonics of W_m--that is, as a Fourier series. The output of the lock-in amplifier is proportional to the coefficient of the fundamental frequency (i. e. W_m) in the Fourier representation. Let this Fourier coefficient be represented by $f(H_0)$, given by Andrew[66] as

$$f(H_0) = \sum_{q=0}^{\infty} c_q \left(\frac{d^{2q+1} g(H)}{d H^{2q+1}} \right)_{H_0} , \qquad \text{where}$$

$$c_q = \frac{H_m^{2q+1}}{2^{2q} \, q! \, (q+1)!} .$$

Applying a double integral gives

$$\int_{-\infty}^{+\infty} \int_{-\infty}^{+\infty} f(H_0) \, d H_0^2 = H_m \int_{-\infty}^{+\infty} g(H) \, d H + \sum_{q=1}^{c} \frac{dg(H)}{dH} \Bigg|_{-\infty}^{+\infty} + \sum_{q=2}^{\infty} c_q \frac{d^q g(H)}{dH^q} .$$

The desired relationship is $\int_{-\infty}^{+\infty}\int_{-\infty}^{+\infty} f(H_0)\, d\, H_0^2 = H_m \int_{-\infty}^{+\infty} g(H)\, d\, h,$

therefore the rest of the terms need to be 0. It is obvious that all the derivatives from the first on in this series are $\equiv 0$ for Lorentzian $\left(g(H_0) = \frac{1}{A+H_0^2} \right)$ and Gaussian $\left(g(H_0) = \frac{k}{(\pi)^{1/2} k^2 H_0^2} \right)$ shape functions. Stating this requirement as a restriction on the shape functions to which this method may be applied, would be a more complex mathematical problem and will not be attempted.

Similarly, applying the method of the first moment gives, on integration by parts,

$$\int_{-\infty}^{+\infty} H_0\, f(H_0)\, d\, H_0 = -\int_{-\infty}^{+\infty}\int_{-\infty}^{+\infty} f(H_0)\, d^2 H_0 + H_0 \int_{-\infty}^{+\infty} f(H_0)\, d\, H_0 \quad .$$

The double-integral term is opposite in sign but otherwise identical to the double-integral treatment just discussed. The third term gives rise to a series of terms

$$H_0 \sum_{q=0}^{\infty} c_q \frac{d^{2q} g(H)}{d\, H^{2q}} \Bigg|_{-\infty}^{+\infty} =$$

$$H_0\, H_m\, g(H) \Big|_{-\infty}^{+\infty} + H_0 \sum_{q=1}^{c} \frac{d^2 g(H)}{d\, H^2} \Bigg|_{-\infty}^{+\infty} + H_0 \sum_{q=2}^{\infty} c_q \frac{d^{2q} g(H)}{d\, H^{2q}} \quad .$$

As before it is obvious that all the terms are 0 for Lorentzian and Gaussian shapes. Again to state the convergence requirements for a general shape function would be difficult. It is apparent that it would be somewhat more severe as we have a term in H_0 as a multiplier of the whole series.

APPENDIX 5

Application of the AAI Method to Lorentzian and Gaussian Shape Functions

Lorentzian Case	Gaussian Case
$g(H) = \frac{1}{1 + A H^2}$	$g(H) = \frac{k}{\sqrt{\pi}} \; e^{-k^2H^2}$
$g'(H) = - \frac{2 A H}{(1+AH^2)^2} = - 2 A H g^2(H)$	$g'(H) = \frac{-2 k^3}{\sqrt{\pi}} H e^{-k^2h^2} = - 2 k^2 H g(H)$
$g''(H) = - 2 A g^2(H) + 8 A^2 H^2 g^3(H)$	$g''(H) = g(H) [- 2 k^2 + (2 k^2 H)^2]$
g'_{max} is determined by $g'' = 0$	$g'_{max}(h)$ determined by $g'' = 0$
$0 = 1 - 4 A g(H) H^2$ or $H^2 = \frac{1 + A H^2}{4 A}$ or	
g' is a maximum at	g' is a maximum at
$(H)_{g'_{max}} = \frac{1}{\sqrt{3A}}$	$(H)^2_{g'_{max}} = \frac{1}{2k^2}$ $\quad H_{g'_{max}} = \frac{1}{k\sqrt{2}}$
$g'_{max} = -2 A \frac{1}{\sqrt{3A}} \left(\frac{1}{1 + \frac{A}{3A}} \right)^2 = - \frac{3\sqrt{3A}}{8}$	$g'_{max} = - \frac{2k^2 k}{k\sqrt{2\pi}} e^{\frac{-k^2}{2k^2}} = - \frac{\sqrt{2} k^2}{\sqrt{\pi e}}$
$AAI = g'_{max}(2H)^2_{g'_{max}} = \frac{\sqrt{3}}{2\sqrt{A}}$	$AAI = - k^2 \sqrt{\frac{2}{\pi e}} \left(\frac{2}{\sqrt{2}k} \right)^2 = \frac{2\sqrt{2}}{\sqrt{\pi e}} = 0.97$
since $\int_{-\infty}^{+\infty} g(H)\, dH = \int_{-\infty}^{+\infty} \frac{dH}{(1 + A H^2)} = \frac{\pi}{\sqrt{A}}$	since $\int_{-\infty}^{+\infty} g(H)\, dH = \int_{-\infty}^{+\infty} \frac{k}{\sqrt{\pi}} e^{-k^2H^2} dH = 1.00$
$\frac{\text{actual area}}{AAI} = 3.64$	$\frac{\text{actual area}}{AAI} = \frac{1.00}{0.97} = 1.03$

LIST OF ILLUSTRATIONS

LIST OF TABLES

LIST OF MECHANISMS

BIBLIOGRAPHY

1. Tolbert, Adams, Bennett, Hughes, Kirk, Lemmon, Noller, Ostwald, and Calvin, J. Am. Chem. Soc. 75, 1867 (1953).
2. B. M. Tolbert and R. M. Lemmon, Radiation Research 3 52 (1955).
3. E. Collinson and A. J. Swallow, Chem. Revs. 56, 471 (1956).
4. Ernest B. A. Baldwin, Ph. D., Dynamic Aspects of Biochemistry (Cambridge University Press, 1949).
5. Benjamin Harrow, Ph. D., Text Book of Biochemistry, (W. B. Sanders and Company, Philadelphia 1946.)
6. Lemmon, Gordon, Parsons, and Mazzetti, J. Am. Chem. Soc. 80, 2730 (1958).
7. I. Serlin, Science 126, 261 (1957).
8. R. L. Collin, J. Am. Chem. Soc. 79, 6086 (1957).
9. B. M. Tolbert, Elmer Nielson, George Edwards, I. M. Whittemore and N. B. Gordon, in Chemistry Division Quarterly Report, UCRL-3710, March 1957, p. 72.
10. R. M. Lemmon and D. F. Mosier, Radiation Research 4, 323 (1956).
11. D. Glick, J. Biol. Chem. 156, 643 (1944).
12. P. Marquardt and G. Vogg. Z. physiol. Chem., Hoppe-Seyler's 291, 143 (1952).
13. F. Halverson, Revs. Modern Phys. 19, 87 (1947).
14. H. J. Bernstein, Can. J. Chem. 29, 284 (1951).
15. R. Livingstone, H. Zeldes, and E. H. Taylor, Phys. Rev. 96, 1702 (1954).
16. Max S. Matheson and B. Smaller, J. Chem. Phys. 23-3, 521 (1955).
17. R. S. Alger, T. H. Anderson, and L. A. Webb, J. Chem. Phys. 30-3, 695 (1959).
18. F. C. Adam and S. I. Weissman, J. Am. Chem. Soc., 802, 2057 (1958).
19. M. Adams, M. S. Blois, and R. H. Sands, J. Chem. Phys. 28, 1169 (1958).
20. W. Gordy, W. B. Ard, and H. Shields, Proc. Natl. Acad. Sci. U.S. 41, 983 (1955).
21. B. Smaller and M. S. Matheson, J. Chem. Phys. 28, 1169 (1958).

22. Arthur Murray III and D. L. Williams, Organic Syntheses with Isotopes (Interscience Publishers, Inc., New York, 1958).
23. H. R. V. Arnstein and R. Bently, Quarterly Reviews IV-2, 172 (1950).
24. S. L. Thomas and H. S. Turney, Quarterly Reviews VII-4, 19 (1952).
25. L. M. Brown and A. S. Freedman, "Biblography of Deuterium and Tritium Compounds", National Bureau of Standards.
26. R. L. Dannley, M. Lukin, and J. Shapiro, J. Org Chem. 20, 92-94 (1955).
27. Hill, Judge, Skell, Kantor, and Hauser, J. Am. Chem. Soc. 74, 5599 (1952).
28. C. L. Wilson, J. Chem. Soc. 1935, 492.
29. O. Diels and B. Wolf, Ber. deut. chem. Ges. 39, 689 (1906).
30. C. C. Hurd and F. D. Pilgrim, J. Am. Chem. Soc. 25, 757 (1933).
31. Merck and Co., Ltd., P. O. Box 899, Montreal 3, Quebec, Canada; Isotope Specialties Co., 703 South Main St., Burbank, California.
32. Jacob Kleinberg, Chem. Revs. 46, 381 (1947).
33. W. G. Dauben and H. Tilles, J. Am. Chem. Soc. 72, 3185 (1947).
34. J. F. Arens and D. A. Van Dorp, Rec. trav. chim. 66, 409 (1947).
35. O. Vogl and M. Pohn, Monatsh, Chem. 83, 541-543 (1952).
36. T. Habgood, L. Marion, and H. Shwarz, Helv. Chim. Acta 35, 638 (1952).
37. R. Willstätter, Ber. deut. chem. Ges. 35, 595 (1902).
38. E. F. Zavoisky, Phys. U.S.S.R. 9, 211 (1945).
39. R. Livingston, H. Zeldes, and E. H. Taylor, Phys. Rev. 96, 1702 (1954).
40. S. I. Weissman and D. Banfill, J. Am. Chem. Soc. 75, 2534 (1953).
41. J. E. Wertz and J. L. Vivo, J. Chem. Phys. 23, 2441 (1955).
42. M. Adams, M. S. Blois, and R. H. Sands, J. Chem. Phys. 28, 774 (1958).
43. R. J. Abraham and D. H. Whiffen, Trans. Faraday Soc. 54, 1291 (1958).

44. N. M. Atherton, H. W. Melville, and D. H. Whiffen, Trans. Faraday Soc. 54, 1300 (1958).
45. C. F. Luck and W. Gordy, J. Am. Chem. Soc. 78, 3240 (1956).
46. W. Gordy and C. G. McCormick, J. Am. Chem. Soc. 78, 3243 (1956).
47. W. R. McDonnell and A. S. Newton, J. Am. Chem. Soc. 76, 4561 (1954).
48. W. Gordy, W. B. Ard, and H. Shields, Proc. Natl. Acad. Sci. U. S. 41, 983 (1955).
49. G. McCormick and W. Gordy, J. Phys. Chem. 62, 783 (1958).
50. D. J. E. Ingram, Free Radicals as Studied by Electron Spin Resonance (Academic Press, New York, 1958), p. 103.
51. B. Fingerman and R. M. Lemmon, in Bio-Organic Chemistry Quarterly Report, UCRL-8698, March 1959, p. 13.
52. D. J. E. Ingram, Spectroscopy at Radio and Microwave Frequencies (Philosophical Library, New York, 1956), p. 100.
53. J. E. Wertz, Chem. Revs. 55, 918 (1955).
54. D. M. Gardner and B. F. Fraenkel, J. Am. Chem. Soc. 78, 3279 (1956).
55. E. A. Braude, A. G. Brook, and R. P. Linstead, J. Chem. Soc. 3574, (1954).
56. R. H. Poerie, F. J. Kahler, and F. Benington, J. Org. Chem. 17, 1437 (1952).
57. Eastman Kodak Co., Catalog No. 41 compound No. 7356.
58. Aldrich Chemical Co., Catalog No. 8.
59. R. H. Silsbee, Phys. Rev. 103, 1675 (1956).
60. W. Low, Ann. N. Y. Acad. Sci. 72, 69-126 (1958).
61. D. W. Hershberger and H. N. Leifer, Phys. Rev. 88, 714 (1952).
62. Periclase is available from Infrared Development Co., Welwyn Garden City, England, according to a private communication from Prof. John E. Wertz.
63. A. Bose, Proc. Indian Acad. Sci. 1A, 605 (1935).
64. D. J. Ingram, Free Radicals as Studied by Electron Spin Resonance, (Academic Press, Inc., New York, 1958), p. 28.

65. E. R. Andrew, Phys. Rev. 91, 425 (1953).

66. G. E. Pake and E. M. Purcell, Phys. Rev. 74, 1184 (1948).

67. R. M. Lemmon, M. A. Parsons, and D. M. Chin, J. Am. Chem. Soc. 77, 4139 (1955).

68. G. J. Dienes and G. H. Vineyard, Radiation Effects in Solids Interscience Publishers, In., New York, (1957), p. 51 and 64.

69. M. E. Senko, The Crystal Structure of a Triazole and Choline Chloride, UCRL-3521, Sept. 1956, p. 21.

70. F. O. Rice and K. F. Herzfeld, J. Am. Chem. Soc. 56, 284 (1934).

71. K. Wiberg, Chem. Revs. 55-4, 713 (1955).

72. G. Friedlander and J. W. Kennedy, Nuclear and Radiochemistry (John Wiley and Sons, New York, 1955), p. 203.